Infections are not alike: the effects of covariation between individual susceptibility and transmissibility on epidemic dynamics

Jeremy D. Harris[1,§,†,✉], Esther Gallmeier[2,‡], Stephen J. Beckett[3,†], Joshua S. Weitz[3,4,†,✉]

1 Department of Mathematics, Spelman College, Atlanta, GA, USA
2 Center for Applied Mathematics, Cornell University, Ithaca, NY, USA
3 Department of Biology, University of Maryland, College Park, MD, USA
4 Institut de Biologie, École Normale Supérieure, Paris, France

prior addresses:
§ Department of Mathematics, Rose-Hulman Institute of Technology, Terre Haute, IN, USA
† School of Biological Sciences, Georgia Institute of Technology, Atlanta, GA, USA
‡ School of Mathematics, Georgia Institute of Technology, Atlanta, GA, USA

Corresponding Authors:
✉Jeremy D. Harris: E-mail: jeremy.harris31@gmail.com
✉Joshua S. Weitz: E-mail: jsweitz@umd.edu

keywords: *Epidemiology, Individual Variation, Heterogeneity, Susceptibility, Transmissibility, Nonlinear dynamics*

Highlights:

- Developed models incorporating susceptibility and transmissibility covariation.[**SJB:** *79 char*]
- Identified gamma and Gaussian eigendistributions of the force of infection. [**SJB:** *75*]
- Uncorrelated transmissibility reduces to variation in susceptibility alone (mean transmissibility constant). [**JDH:** *108*]
- Positive correlations give faster, stronger, more likely outbreaks (β, γ fixed). [**JDH:** *93*]
- Positive correlations lead to slower, weaker outbreaks ($\mathcal{R}_0$ fixed). [**JDH:** *79*]
- Positive correlations & overdispersed transmission may reduce the effective transmission over time. [**JDH:** *100*]

[**SJB:** *note only meant to be 3-5 highlights, each max of 85 characters long - many too long!*]

Abstract

Individual-level variation in susceptibility to infection and transmissibility of infection can affect population-level dynamics in epidemic outbreaks. Prior work has incorporated variation in susceptibility or transmissibility of individuals into epidemic models independently. Here, we provide a mathematical framework that includes covariation in susceptibility and transmissibility. First, we show that uncorrelated variation in susceptibility and transmissibility leads to an effective transmissibility distribution that has a constant coefficient of variation such that the epidemic dynamics match those with variation in susceptibility alone, providing a baseline for comparison across different correlation structure. Importantly, increasing the correlation between susceptibility and transmissibility increases both the speed and strength of the outbreak. Mechanistically,

correlations can shift the transmissibility distribution, thereby modifying the speed of the epidemic as the susceptible population is depleted. Finally, we show how overdispersion in transmissibility with positive correlations affects epidemic progression – the overdispersed transmission rates decrease over time as the epidemic progresses due to the rapid depletion of highly transmissible individuals earlier in the epidemic. Overall, this work demonstrates how (often unaccounted) covariation in susceptibility and transmission can shape the course of outbreaks and final outbreak sizes.

1 Introduction

Individuals differ in response to infection: some people may be more likely to get sick than others, and some people may be more likely to transmit an infection on to others. Variation in susceptibility to infection has been introduced into susceptible-infectious-recovered (SIR) (and related) compartmental epidemic models (Kermack & McKendrick, 1927) to account for intrinsic heterogeneity (Rose et al., 2021; Gomes et al., 2022), extrinsic differences based on, e.g., age-dependent contact rates (Davies et al., 2020; Lovell-Read et al., 2022), or differences in prior immunity (Gart, 1972). Prior research has found that variation in susceptibility reduces the epidemic burden (i.e., outbreak size) relative to the homogeneous model (Ball, 1985; Dushoff & Levin, 1995; Coutinho et al., 1999; Dwyer et al., 2000; Novozhilov, 2008; Novozhilov, 2012; Karev & Novozhilov, 2019; Britton et al., 2020; Rose et al., 2021; Gomes et al., 2022; Tuschhoff & Kennedy, 2024). Hence, the distribution of heterogeneity in susceptibility and the epidemic burden can jointly vary: when susceptible individuals become infected, the joint variation leads to the redistribution and 'sculpting' of the susceptibility distribution. The sculpting leads to epidemic slowdowns relative to that of the homogeneous case, reflecting a fundamental difference in the nonlinearity of incident infections in the model. As shown in Rose et al., 2021, the susceptibility distribution is sculpted toward eigendistributions e.g., gamma distributions with constant coefficient of variation. Hence, outbreaks may appear similar during the early stages, but heterogeneity in susceptibility can slow the speed of the epidemic, leading to lower final outbreak sizes (Rose et al., 2021; Gomes et al., 2022).

Variability in transmission has also been studied in epidemic models. For instance, variation in the number of secondary cases caused by a particular infected individual may be common in diseases transmitted by non-sexual direct contacts, such as SARS-CoV-2 or smallpox (Lloyd-Smith et al., 2005; Meehan et al., 2023) in addition to sexually transmitted disease e.g., Murayama et al., 2023. During the COVID-19 pandemic, household surveys suggest significant variation in both susceptibility and transmissibility (Anderson et al., 2023); and contact survey data has shown that age-dependent variation in contact rates can be a key driver of variation in transmission (Zhang et al., 2020) and susceptibility (Britton et al., 2020). Variation in susceptibility and transmissibility has previously been introduced to epidemic compartmental models. For instance, in a parasite-host system, susceptibility values were fit to dose-response data; they showed that the transmission rate is lower with more heterogeneity (Dwyer et al., 1997). Additionally, models with uncorrelated variation in susceptibility and transmissibility have previously been developed and explored – showing that powerlaw distributions in transmission can arise from initial gamma distributed susceptibility and transmissibility (Novozhilov, 2012). [**JDH:** *SIAM - networks with correlated in and out degrees (Allard et al., 2023)*]

Hence, variation in susceptibility and transmissibility can both shape disease dynamics, but compartmental epidemic models have yet to generalize for the effects of potential covariation on the epidemic dynamics. For example, individuals who interact more with others may be more likely to become infected and more likely to infect others (e.g., if they continue to interact at similar rates when infectious). Likewise, individuals may be more vulnerable to infection due to health/genetic factors that mean they have limited interactions when infectious (e.g., with trained health-care providers) and are therefore less likely to infect others. In this manuscript, we provide a mathematical framework that includes individual-level variation in both susceptibility and transmissibility. The framework allows for comparisons between different model implementations of variation in susceptibility and transmissibility and makes explicit the consequences of covariation between susceptibility and

transmissibility on outbreak dynamics.

2 Model Framework

2.1 Epidemiological dynamics of models with susceptibility and transmissibility

We extend the model framework developed in Rose et al., 2021 to incorporate heterogeneity in both susceptibility and transmissibility into SIR-like epidemic models. To do so, we consider the following population compartment states: susceptible (S), infected (I), and recovered (R). We assume that each individual in the population has a fixed intrinsic susceptibility value, ε, as well as fixed intrinsic transmissibility value, δ. Hence, the S-I-R compartments are functions of susceptibility (ε) and transmissibility (δ) such that $S(t,\varepsilon,\delta)$, $I(t,\varepsilon,\delta)$, and $R(t,\varepsilon,\delta)$. We denote $S(t)$, $I(t)$, $R(t)$ to represent the respective population densities of all susceptible, infected and recovered individuals. Then we can define sub-population densities: the susceptible population density with intrinsic susceptibility ε and intrinsic transmissibility δ is given by

$$f_S(t,\varepsilon,\delta) = \frac{S(t,\varepsilon,\delta)}{S(t)}\,, \tag{1}$$

the infected population density is

$$f_I(t,\varepsilon,\delta) = \frac{I(t,\varepsilon,\delta)}{I(t)}\,, \tag{2}$$

and the recovered population density is

$$f_R(t,\varepsilon,\delta) = \frac{R(t,\varepsilon,\delta)}{R(t)}\,. \tag{3}$$

Note that these definitions are joint densities such that at any time, t, then $\int_0^\infty \int_0^\infty f_S(t,\varepsilon,\delta)\,d\varepsilon\,d\delta = \int_0^\infty \int_0^\infty f_I(t,\varepsilon,\delta)\,d\varepsilon\,d\delta = \int_0^\infty \int_0^\infty f_R(t,\varepsilon,\delta)\,d\varepsilon\,d\delta = 1$. To calculate the mean susceptibility and transmissibility over time, we consider the marginal distributions relevant to the disease dynamics:

$$g_S(t,\varepsilon) := \int_0^\infty f_S(t,\varepsilon,\delta)\,d\delta \quad \text{(Susceptibility Distribution)} \tag{4}$$

$$h_I(t,\delta) := \int_0^\infty f_I(t,\varepsilon,\delta)\,d\varepsilon \quad \text{(Effective Transmissibility Distribution)}\,. \tag{5}$$

The other relevant marginal distribution is the potential transmissibility distribution in the susceptible population, indicative of the remaining infectivity of the population who might be infected in the future, which is given by:

$$h_S(t,\delta) = \int_0^\infty f_S(t,\varepsilon,\delta)\,d\varepsilon \quad \text{(Potential Transmissibility Distribution)}\,. \tag{6}$$

During the exponential growth phase of the epidemic, individuals are drawn from the susceptible population at varying rates that depend on an individual's susceptibility to infection. As individuals become infected, their contribution to *effective* transmissibility is drawn from the *potential* transmissibility distribution, and thus, the *effective* transmissibility distribution (Equation 5) is "filled in" by the *potential* transmissibility distribution given in Equation 6.

Given the susceptibility distribution (Equation 4) and transmissibility distributions (Equations 5-6), we can define the mean susceptibility and transmissibility. The mean susceptibility to infection within the susceptible population is:

$$\bar{\varepsilon}(t) = \int_0^\infty \varepsilon\, g_S(t,\varepsilon)\,d\varepsilon\,, \tag{7}$$

the mean *effective* transmissibility of individuals within the infected population is:

$$\bar{\delta}_I(t) = \int_0^\infty \delta\, h_I(t,\delta)\, d\delta\,, \tag{8}$$

and the mean *potential* transmissibility of individuals in the susceptible population is:

$$\bar{\delta}_S(t) = \int_0^\infty \delta\, h_S(t,\delta)\, d\delta\,. \tag{9}$$

Then the force of infection to the susceptible population with susceptibility level ε is:

$$\lambda(t,\varepsilon) = \beta\, I(t)\, \bar{\delta}_I(t)\, \varepsilon\,, \tag{10}$$

where β is the baseline transmission rate. For each subpopulation with (ε, δ), the SIR model equations with susceptibility and transmissibility heterogeneity can be written as:

$$\begin{aligned}
\frac{\partial S(t,\varepsilon,\delta)}{\partial t} &= -\lambda(t,\varepsilon)\, S(t,\varepsilon,\delta) \\
\frac{\partial I(t,\varepsilon,\delta)}{\partial t} &= \lambda(t,\varepsilon)\, S(t,\varepsilon,\delta) - \gamma\, I(t,\varepsilon,\delta) \\
\frac{\partial R(t,\varepsilon,\delta)}{\partial t} &= \gamma\, I(t,\varepsilon,\delta)\ ,
\end{aligned} \tag{11}$$

where γ is the recovery rate of all infected individuals. See Appendix A for the derivation of Equation 11 from discrete model variables. See Figure 1 for a visual representation of the model framework using discrete susceptibility and transmissibility variables.

Integrating with respect to the continuous variables, ε and δ, we can obtain the total population incidence:

$$\eta(t) = \beta\, \bar{\delta}_I(t)\, I(t)\, \bar{\varepsilon}(t)\, S(t)\ . \tag{12}$$

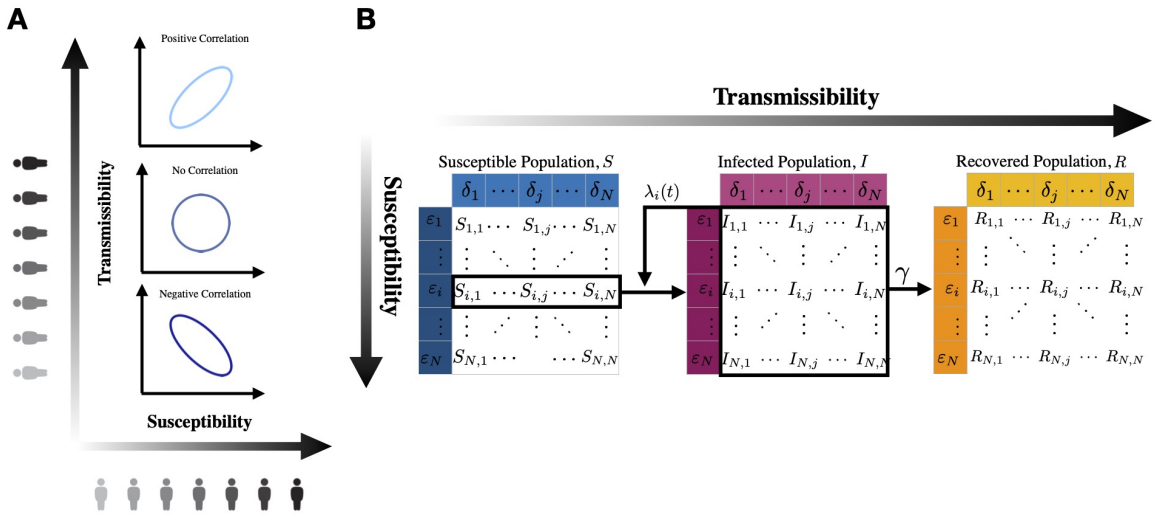

Figure 1. Model diagram: susceptible (S), infected (I), and recovered (R) populations with individual variation in susceptibility and transmissibility. (A) Positive correlation, no correlation, and negative correlation between individual susceptibility and transmissibility. **(B)** S-I-R compartments are discretized into subpopulations distributed according to susceptibility (ε_i) and transmissibility (δ_j). Here, $\lambda_i(t) = \lambda(t, \varepsilon_i)$ is the force of infection to the susceptible population with susceptibility, ε_i, and γ is the mean recovery rate for all infected individuals.

From here, differential equations for the following variables can be identified: the mean susceptibility ($\bar{\varepsilon}(t)$); the mean potential transmissibility ($\bar{\delta}_S(t)$); and the mean effective transmissibility ($\bar{\delta}_I(t)$). This reduced model can be described by the following 6-dimensional system of ordinary differential equations:

$$\begin{aligned}
\dot{S} &= -\beta\,\bar{\delta}_I I\,\bar{\varepsilon}\,S \\
\dot{I} &= \beta\,\bar{\delta}_I I\,\bar{\varepsilon}\,S - \gamma\,I \\
\dot{R} &= \gamma\,I \\
\dot{\bar{\varepsilon}} &= -\beta\,\bar{\delta}_I I \sigma_\varepsilon^2(t) \\
\dot{\bar{\delta}}_S &= -\beta\,\bar{\delta}_I I\,\left(\bar{M}_S(t) - \bar{\varepsilon}\,\bar{\delta}_S\right) \\
\dot{\bar{\delta}}_I &= \beta\,\bar{\delta}_I\,\left(\bar{M}_S(t) - \bar{\varepsilon}\,\bar{\delta}_I\right) S\,.
\end{aligned} \tag{13}$$

Here, the dependence on t is implicit for all time-dependent variables except for the mean of the joint distribution of the susceptible population, indicated by $\bar{M}_S(t) = \mathrm{cov}_S(\varepsilon,\delta)(t) + \bar{\varepsilon}(t)\,\bar{\delta}_S(t)$, (where $\mathrm{cov}_S(\varepsilon,\delta)$ is the covariance between ε and δ in S) and the variance, $\sigma_\varepsilon^2(t)$, of the susceptibility distribution, $g_S(t,\varepsilon)$. This system is not closed for arbitrary starting joint distributions in the susceptible population, as $\bar{M}_S(t)$ and $\sigma_\varepsilon^2(t)$ may change over time, impacting the mean susceptibility and transmissibility as the epidemic progresses.

2.2 Associations of correlations with epidemic strength and dispersion

Using the dynamical system presented in Equation 13, we can define the basic reproduction number ($\mathcal{R}_0$) and dispersion (κ) of epidemics as a function of the correlation coefficient (ρ) between susceptibility and transmissibility. First, in a fully susceptible population, $S = 1$, the basic reproduction number is given by:

$$\mathcal{R}_0 = \frac{\beta}{\gamma}\,\bar{\varepsilon}(0)\,\bar{\delta}_I(0)\,, \tag{14}$$

where $\bar{\delta}_I(0)$ is the mean effective transmissibility during initial exponential growth, and $\bar{\varepsilon}(0)$ is the initial mean susceptibility. Note that without correlations (i.e., $\rho = 0$) between initial susceptibility and transmissibility values, then $\bar{\delta}_I(0) = \bar{\delta}_S(0)$, but with correlations (i.e., $\rho \neq 0$), they can differ. During exponential growth, the joint distribution of the susceptible population is fixed, which implies that the derivatives, $\dot{\bar{\varepsilon}} = \dot{\bar{\delta}}_S = 0$. Hence, both ε and $\bar{\delta}_S$ remain fixed during the exponential growth phase. Since the covariance of the joint distribution of the susceptible population, $\mathrm{cov}_S(\varepsilon,\delta)(t)$, also remains fixed during the exponential growth phase, then $\bar{M}_S(t) = \bar{\varepsilon}(t)\,\bar{\delta}_S(t) + \mathrm{cov}_S(\varepsilon,\delta)(t)$ is constant. Hence, in order to obtain the reproduction number, we need to find $\delta_I(0)$ relative to $\delta_S(0)$. In order for $\dot{\bar{\delta}}_I = 0$ during exponential growth, then $\bar{\delta}_I$ must converge to $\bar{\delta}_I(0) = \left(\bar{\varepsilon}(0)\,\bar{\delta}_S(0) + \mathrm{cov}_S(\varepsilon,\delta)(0)\right)/\bar{\varepsilon}(0)$, and the reproduction number is

$$\mathcal{R}_0 = \frac{\beta}{\gamma}\left(\bar{\varepsilon}(0)\,\bar{\delta}_S(0) + \mathrm{cov}_S(\varepsilon,\delta)(0)\right). \tag{15}$$

Then the reproduction number can be written equivalently as:

$$\mathcal{R}_0 = \frac{\beta}{\gamma}\,\left(\bar{\varepsilon}(0)\bar{\delta}_S(0) + \rho(\varepsilon,\delta)\,\sigma_\varepsilon(0)\,\sigma_\delta(0)\right)\,, \tag{16}$$

where the correlation coefficient between susceptibility and transmissibility (during exponential growth) is given by $\rho(\varepsilon,\delta) = \frac{\mathrm{cov}_S(\varepsilon,\delta)(0)}{\sigma_\varepsilon(0)\sigma_\delta(0)}$.

Second, to define the dispersion, $\kappa(t)$, of an epidemic we first let the mean susceptibility, $\bar{\varepsilon}(t)$, serve as a dimensionless progress variable. Rose et al., 2021 used $\phi(t) = \beta\int_0^t I(s)\,ds = \frac{\beta}{\gamma}R(t)$ as a dimensionless progress variable, noting that $\phi(t)$ is proportional to cumulative infections. We compute

the mean susceptibility ($\bar{\varepsilon}(t)$), potential transmissibility ($\bar{\delta}_S(t)$), and effective transmissibility ($\bar{\delta}_I(t)$) as the epidemic progresses over time. We also compute the variances $\sigma^2_\varepsilon(t)$ and $\sigma^2_\delta(t)$ in order to obtain the corresponding squared coefficients of variation over time.

From Equation 13, we follow the analysis in (Rose et al., 2021) and have that $\frac{d\bar{\varepsilon}}{dS} = \frac{\sigma^2_\varepsilon}{\bar{\varepsilon}\,S}$. Using differential notation, $d(\ln(x)) = dx/x$, then the square of the coefficient of variation for the susceptibility distribution is given by:

$$\kappa(t) = \frac{d(\ln(\bar{\varepsilon}(t)))}{d(\ln(S(t)))} = \frac{\sigma^2_\varepsilon(t)}{\bar{\varepsilon}^2(t)}\,. \tag{17}$$

For given initial distributions, we compute the squared coefficient of variation for the susceptibility distribution as well as the squared coefficients of variation for the potential and effective transmissibility distributions over time.

3 Results

3.1 Uncorrelated gamma-distributed susceptibility and transmissibility

We first examine the dynamics of Equation 13 when susceptibility and transmissibility are uncorrelated. In this case, the covariance is zero so that the mean of the initial joint distribution reduces to the product of the means, $\bar{M}_S(t) = \bar{\varepsilon}(t)\,\bar{\delta}_S(t)$, where $\bar{\varepsilon}(t)$ is mean susceptibility and $\bar{\delta}_S(t)$ is the mean potential transmissibilty in the susceptible population. Hence, from Equation 13, $\dot{\bar{\delta}}_S = 0$ and so $\bar{\delta}_S$ remains constant over time. If the initial potential and effective transmissibility values are equal, i.e., $\bar{\delta}_S(0) = \bar{\delta}_I(0)$, then $\bar{M}_S(0) = \bar{\varepsilon}(0)\,\bar{\delta}_S(0)$, which means that $\dot{\bar{\delta}}_I(0) = \beta\,\bar{\delta}_I\,\bar{\varepsilon}\,\left(\bar{\delta}_S(0) - \bar{\delta}_I(0)\right) S = 0$. Since $\bar{\delta}_S$ is constant, then $\bar{\delta}_I$ remains constant and equal to the initial potential value, $\bar{\delta}_S(0)$. Therefore, without correlations, Equation 13 further simplifies to

$$\begin{aligned}
\dot{S} &= -\beta\,\bar{\delta}_I\,I\bar{\varepsilon}\,S \\
\dot{I} &= \beta\,\bar{\delta}_I\,I\bar{\varepsilon}\,S - \gamma I \\
\dot{R} &= \gamma I \\
\dot{\bar{\varepsilon}} &= -\beta\,\bar{\delta}_I\,I\,\sigma^2_\varepsilon(t)\,.
\end{aligned} \tag{18}$$

This nonlinear dynamical system is equivalent to prior work on variation in susceptibility alone (Rose et al., 2021; Gomes et al., 2022). Here, the variance in susceptibility $\sigma^2_\varepsilon(t)$ is denoted with explicit t to emphasize that it may change over the course of the outbreak. In this work, we introduce a variation of this model, which we term the 'reduced model', in which we set $\sigma^2_\varepsilon(t) = \sigma^2_\varepsilon(0)$.

To examine how the initial distributions changes through the epidemic dynamics, we first consider initially gamma-distributed susceptibility and transmissibility values and examine the squared coefficient of variation in susceptibility, $\kappa(t) = \frac{\sigma^2_\varepsilon}{\bar{\varepsilon}^2}$ (see Equation 17). For initially uncorrelated gamma-distributions, we find that: $\kappa(t) = \frac{\sigma^2_\varepsilon}{\bar{\varepsilon}^2} = \frac{1}{k}$, where k is the shape parameter of the susceptibility distribution, $g_S(0,\varepsilon)$. Here, the mean transmissibility, $\bar{\delta}_I(t)$, is a multiplicative factor that modifies the force of infection. However, since $\bar{\delta}_I(t)$ is constant, the system collapses to the system with variation in susceptibility alone. Hence, initially gamma-distributed susceptibility distributions remain gamma-distributed with mean: $\bar{\varepsilon}(t) = S(t)^{\frac{1}{k}}$ (Rose et al., 2021; Gomes et al., 2022). That is, the same power-law relationship between susceptibility (ε) and the susceptible population ($S(t)$) holds here with uncorrelated gamma-distributed variation in susceptibility and transmissibility.

We can analyze the change in the joint distribution of susceptibility and transmissibility in the susceptible population, $f_S(t,\varepsilon,\delta)$, through the epidemic dynamics. We find that $f_S(t,\varepsilon,\delta)$ satisfies the partial differential equation:

$$\frac{\partial f_S(t,\varepsilon,\delta)}{\partial t} = -\beta\,I\,\bar{\delta}_I\;(\varepsilon - \bar{\varepsilon})\;f_S(t,\varepsilon,\delta)\,. \tag{19}$$

(see Appendix B). Note that we can integrate equation Equation 19 over all transmissibility values so that the marginal susceptibility distribution $g_S(t,\varepsilon)$ satisfies:

$$\frac{\partial g_S(t,\varepsilon)}{\partial t} = -\beta\, I\, \bar{\delta}_I\ (\varepsilon - \bar{\varepsilon})\ g_S(t,\varepsilon)\,, \tag{20}$$

It has been shown (see Section S3 in Rose et al., 2021) that distributions of the exponential family, including initially uncorrelated gamma distributions, with shape parameter k, of the form:

$$g_S(t,\varepsilon) = \left(\frac{k}{\bar{\varepsilon}}\right)^k \frac{\varepsilon^{k-1}}{\Gamma(k)}\, e^{-k\varepsilon/\bar{\varepsilon}} \tag{21}$$

satisfy the PDE given in Equation 20.

To verify this analysis, we can compare the simulations of the discrete model given in Equation 11 with the uncorrelated reduced model in Equation 18. Details of model parameterization and simulation are given in Appendix C-E. For initially uncorrelated gamma-distributed susceptibility and transmissibility, the dynamics of incident infections (Figure 2A, blue) agree with Equation 18 (Figure 2A, green dashed). They also agree with the case of variation in susceptibility alone (Figure 2A, dashed black). Consistent with results of Rose et al., 2021, variation in susceptibility slows down incident infections compared to the classical SIR model (Figure 2A, gray). As predicted, the κ for both susceptibility transmissibility remain constant over time (Figure 2B,C). We show the initial joint distribution, $f_S(0,\varepsilon,\delta)$, in the susceptible population with uncorrelated susceptibility (ε; x-axis) and potential transmissibility (δ; y-axis) (Figure 2D). In Figure 2E, we compare the susceptibility distribution, $g_S(t,\varepsilon)$, at two time points during exponential growth: $t_0 = 0$ days (black circle) and $t_1 = 10$ days (violet circle). The distribution remains constant during exponential growth when susceptible depletion is negligible. In Figure 2F, we show the potential and effective transmissibility distributions at these time points. The epidemic is initialized with a few infected individuals, and the effective transmissibility distribution, $h_I(t,\delta)$, in the infected population is determined by potential transmissibility, $h_S(t,\delta)$, in the susceptible population. Thus, to remove transients, we make the initial transmissibility distributions equal: $h_I(0,\delta) = h_S(0,\delta)$. Then, we show that $h_I(0,\delta) = h_I(t_1,\delta)$ remains fixed during exponential growth (Figure 2F, gray matches dashed violet). These results indicate that initially uncorrelated gamma distributions remain gamma-distributed such that the mean susceptibility satisfies $\bar{\varepsilon}(t) = S(t)^{\frac{1}{k}}$, and the effective mean transmissibility $\bar{\delta}_I$ remains constant such that the transmissibility distribution $h_I(t,\delta)$ is constant over the course of the epidemic.

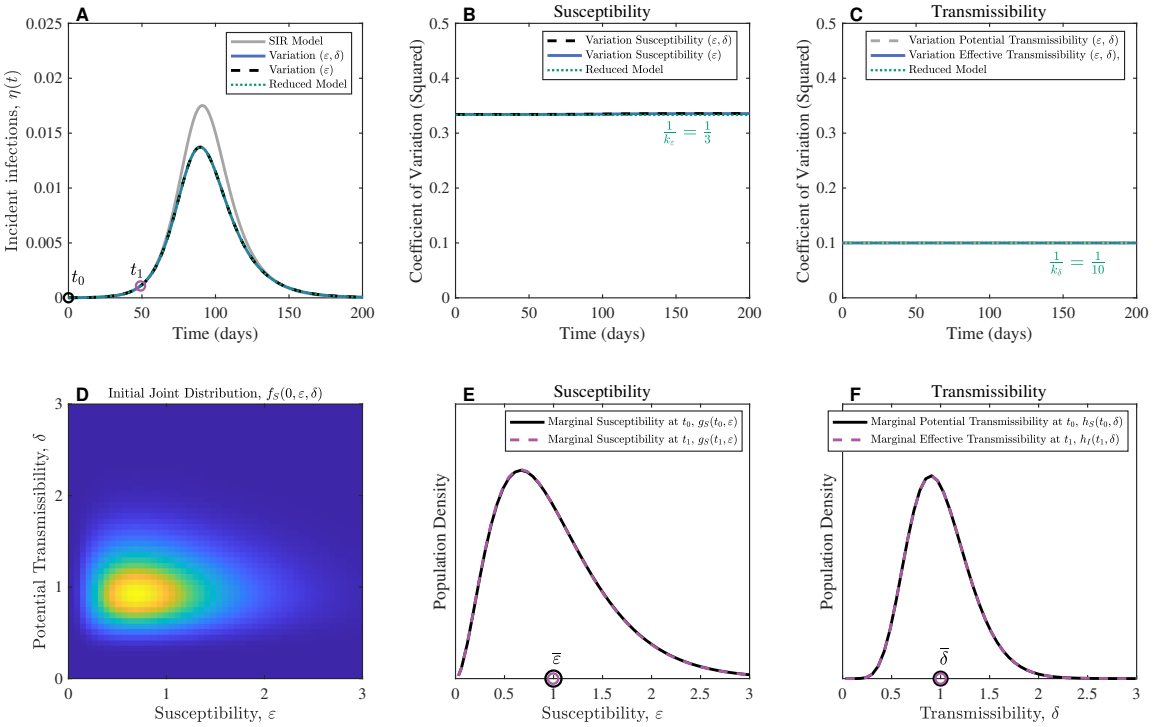

Figure 2. Uncorrelated gamma distributions for susceptibility and transmissibility distributions during exponential growth. **(A)** Incident infections. **(B)** The coefficient of variation (squared) for susceptibility remains constant over time for gamma-distributed susceptibility values. **(C)** The coefficient of variation (squared) in transmissibility remains constant over time for gamma-distributed transmissibility values. **(D)** Initial joint distribution (uncorrelated gamma distributions) for susceptibility values (ε) and potential transmissibility values (δ). **(E)** Comparing Susceptibility distributions at time points: $t_0 = 0$ and $t_1 = 50$ days. **(F)** Potential and effective transmissibility distributions at time points: $t_0 = 0$ and $t_1 = 50$ days. The transmission rate is equal to $\beta = 0.2$, and the recovery rate is equal to $\gamma = 1/10$ such that the basic reproduction number is $\mathcal{R}_0 = 2.0$. Initial gamma distribution shape parameters: $k_\varepsilon = 3$, $k_\delta = 10$. The reduced model refers to Equation 18 with $\sigma_\varepsilon^2(t) = \sigma_\varepsilon^2(0) = 1/k_\varepsilon = 1/3$.

3.2 Uncorrelated Gaussian-distributed susceptibility and transmissibility

As a prelude to introducing correlations we consider initially uncorrelated Gaussian distributions. We show incident infections from discrete model simulations (using Equation 11) in Figure 3A. The coefficient of variation (squared) for susceptibility is constant during the initial exponential growth phase of the outbreak, but increases during susceptible depletion because the mean decreases faster than the variance (see Figure 3B). Here, we set $\sigma_\varepsilon(t) = \sigma_\varepsilon(0)$ in simulations of the reduced model (using Equation 18) and observe increases in $\kappa(t)$ (Figure 3B), meaning that the mean susceptibility decreases. As predicted by our analysis, in reducing Equation 13 in the absence of covariation to Equation 18, the coefficient of variation (squared) for transmissibility remains constant over time (Figure 3C). Despite the differences in κ of susceptibility between the full and reduced models, the reduced model can still approximate incident infections. Consistent with results from Rose et al., 2021, Gaussian and gamma distributions are eigendistributions with respect to the epidemic dynamics. Moreover, gamma distributions have constant κ, whereas Gaussian distributions have constant variance (approximately, considering that Gaussian distributions have proper support on the whole real line).

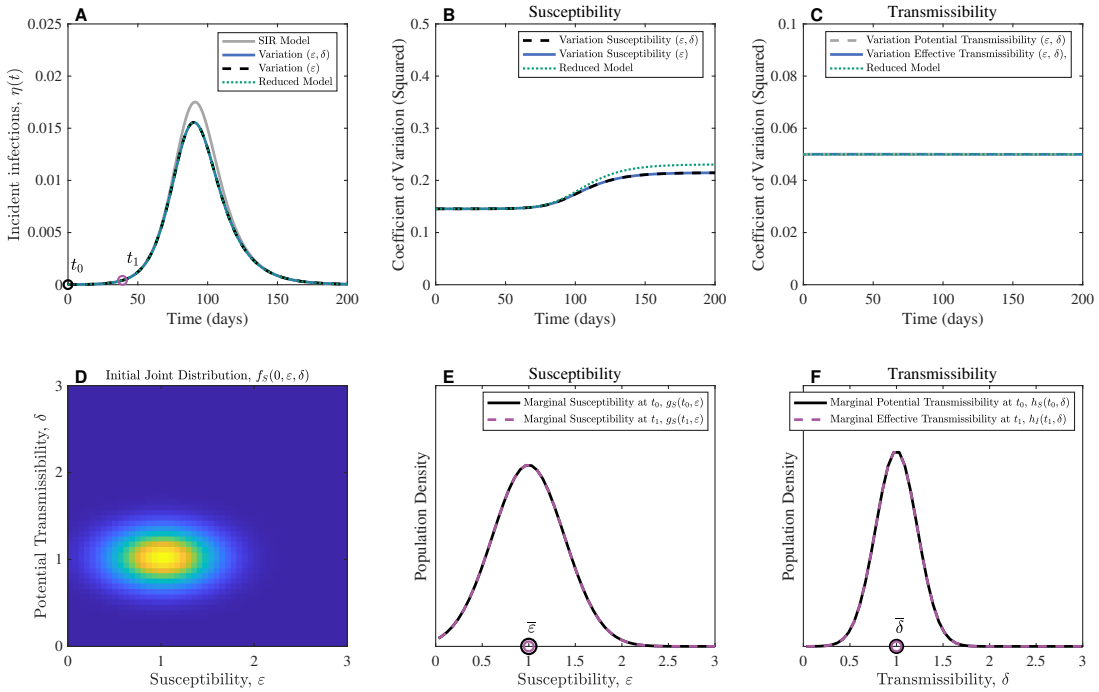

Figure 3. Uncorrelated (low variance) Gaussian distributions for susceptibility and transmissibility during exponential growth. Population dynamics with variation in susceptibility and transmissibility. **(A)** Incident infections. **(B)** Coefficient of Variation (squared) in susceptibility remains constant during exponential growth and increases over time as the susceptible population decreases. **(C)** When transmissibility and susceptibility are uncorrelated, Coefficient of Variation (squared) in transmissibility remains constant over time for Gaussian distributions. **(D)** Initial joint distributions (uncorrelated Gaussian distributions) of susceptibility values (ε) and potential transmissibility values (δ). **(E)** Susceptibility distributions remain constant during exponential growth, shown at two time points: $t_0 = 0$ and $t_1 = 50$ days. **(F)** Potential and effective transmissibility distributions at the time points: $t_0 = 0$ and $t_1 = 50$ days. The transmission rate is equal to $\beta = 0.2$, and the recovery rate is equal to $\gamma = 1/10$ such that the basic reproduction number is $\mathcal{R}_0 = 2.0$. The variance values in the initial joint: $\sigma^2_\varepsilon(0) = 0.15$, $\sigma^2_\delta(0) = 0.05$. The reduced model refers to Equation 18 with $\sigma^2_\varepsilon(t) = \sigma^2_\varepsilon(0) = 0.15$.

To better see the effects of correlations when incorporated, we first increase the variance for both the initial potential susceptibility and transmissibility distributions ($\sigma^2_\varepsilon(0)$ from 0.15 to 0.5; and $\sigma^2_\delta(0)$ from 0.05 to 0.35). Even when the initial variances are increased, we can see reasonable agreement, albeit less than with smaller variance, between the full and reduced model simulations (Figure 4A). For truncated Gaussian initial distributions, the κ in the reduced model simulations increase more than in the discrete model simulations (Figure 4B). [**SJB:** *Due to truncation susceptibility variance decreases over time as well as the mean susceptibility. The reduced model κ diverges as this model is unable to capture this decrease in variance over time, as by definition $\sigma^2_\varepsilon(t) = \sigma^2_\varepsilon(0)$.*] Despite this, the reduced model in Equation 18 still provides a reasonable approximation of incident infections in the discrete model simulations with the highest discrepancies observed during the decay phase (Figure 4A).

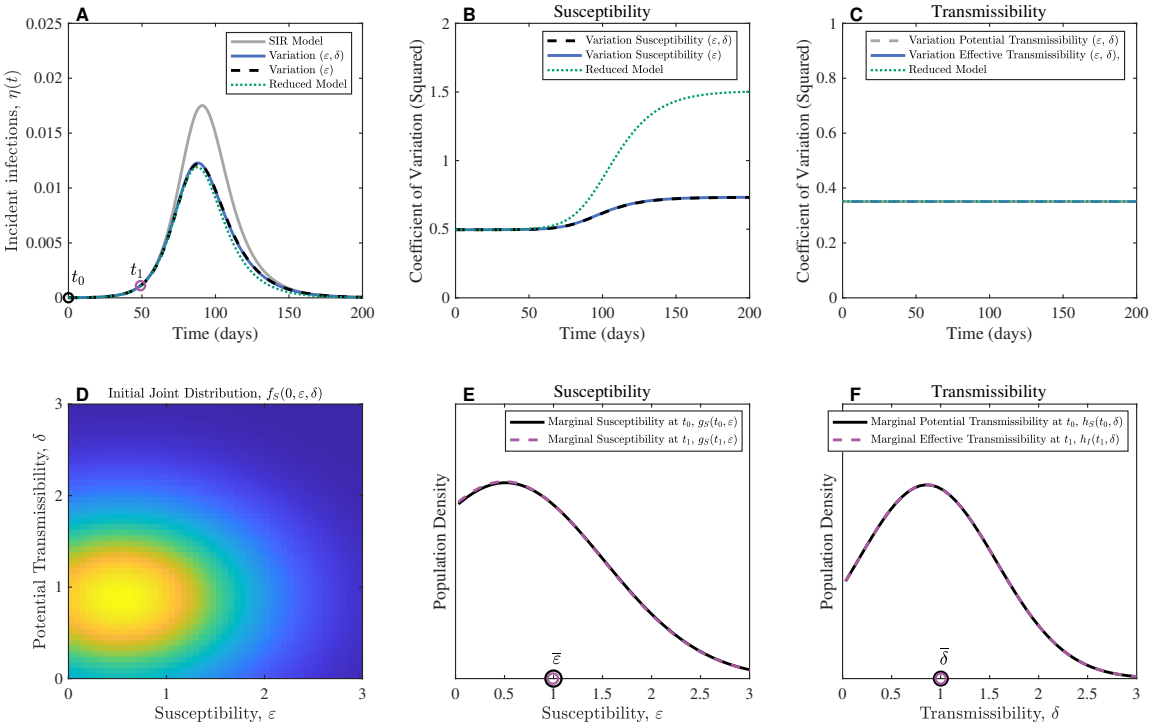

Figure 4. Uncorrelated (high variance) Gaussian distributions for susceptibility and transmissibility during exponential growth. Similar to Figure 3 but with higher variances in the initial susceptibility and transmissibility distribution. **(A)** Incident infections. **(B)** κ for susceptibility. **(C)** κ for transmissibility. **(D)** Initial joint distribution of susceptibility and transmissibility in the susceptible population, $f_S(t_0, \varepsilon, \delta)$, is given by uncorrelated Gaussian distribution, truncated to have positive support in both ε and δ. **(E)** Susceptibility distributions at t_0 and t_1. **(F)** Potential transmissibility distribution at t_0 matches the Effective transmissibility distribution during exponential growth at t_1. Parameters: The transmission rate is $\beta = 0.2$, and the recovery rate is $\gamma = 1/10$ such that the basic reproduction number is $\mathcal{R}_0 = 2.0$. The variance values in the initial joint: $\sigma^2_\varepsilon(0) = 0.50$, $\sigma^2_\delta(0) = 0.35$. The reduced model refers to Equation 18 with $\sigma^2_\varepsilon(t) = \sigma^2_\varepsilon(0) = 0.15$.

3.3 Correlations between susceptibility and transmissibility modify the basic reproduction number

Next, we introduce covariation by considering correlations between susceptibility and transmissibility and compare this against the uncorrelated case. We vary the correlation coefficient (ρ) from negative to positive, in simulations we explore scenarios over the range of values from -0.6 to 0.6, and find that the speed, i.e., the exponential growth rate, increases with increasing correlation (Figure 5A). Recall that the basic reproductive number is dependent on the correlations between susceptibility and transmissibility (Equation 16). In the absence of correlations ($\rho = 0$), the basic reproduction number is $\mathcal{R}_0 = \beta\,\bar{\varepsilon}(0)\,\bar{\delta}_S(0)/\gamma$, and the product of the initial mean susceptibility and transmissibility multiply the basic reproduction of the classic SIR model, β/γ. Note that $\mathcal{R}_0$ is an increasing function of the correlation coefficient, ρ, which is in agreement with simulations (Figure 5B). For $\rho > 0$, the more susceptible individuals are infected earlier and are also more transmissible than on average, causing more transmission during exponential growth such that the basic reproduction number is greater than in the uncorrelated case. For $\rho < 0$, the basic reproduction number is less than in the uncorrelated case because the more susceptible individuals are less transmissible on average (Figure 5B). For a given transmission rate, β, and recovery rate, γ, the initial speed and strength of the epidemic

increases with the initial correlation coefficient between susceptibility and transmissibility, leading to larger outbreaks by larger initial correlation coefficients (Figure 5A).

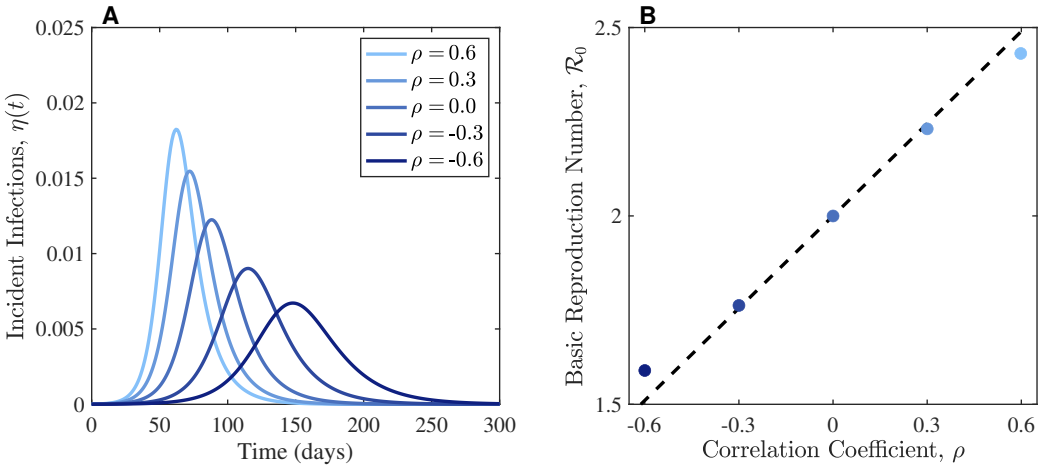

Figure 5. The effects of correlations on the speed and strength of the epidemic. (A) The speed of incident infections is the exponential growth rate which varies with the initial correlation coefficient. Positive correlations between susceptibility and transmissibility result in faster epidemic speeds with increased peak incident infections. **(B)** The basic reproduction increases with increasing initial correlation coefficient. Comparison of Equation 14 with computed $\bar{\delta}_{I,0}$ for the five simulations (colored dots corresponding to the scenarios in **A**) and Equation 16 with (approximately) fixed initial standard deviations of the initial joint susceptibility distribution (dashed line). Across all simulations, the means of the initial joint in susceptibility (i.e., $\varepsilon_S(0) = \delta_S(0) = 1$), the transmission rate is equal to $\beta = 0.2$, and the recovery rate is equal to $\gamma = 1/10$ so that when there is no correlation between susceptibility and transmissibility ($\rho = 0$), then $\mathcal{R}_0 = 2$, as expected in the classical SIR framework. Varying $\rho = -0.6, -0.3, 0, 0.3, 0.6$, the parameter values of initial joint distribution are given by: $\sigma^2_\varepsilon(0) = [0.44, 0.48, 0.50, 0.48, 0.48]$, $\sigma^2_\delta(0) = [0.27, 0.32, 0.35, 0.33, 0.30]$. See Figure S1 for the corresponding initial joint distributions.

3.4 Sensitivity of heterogeneous model outcomes to an outbreaks index case

The introduction of population variability also raises questions about how the initiation of an outbreak may effect epidemic outcomes – the transmissibility and susceptibility of individuals in the the first chains of infection may have a large effect on how an outbreak takes off. To probe this, we first assess how variation in the initial distribution of the infected population may impact epidemic trajectory and timing; and second, utilize stochastic simulations to additionally assess variation in outbreak occurrence and epidemic trajectories. In Figure 6A, we show two example potentials in susceptibility-transmissibility parameter space that an index infection could take, and examine the impact of these choices on epidemic trajectories in Figure 6B. We find that differences in the transmissibility (but, not susceptibility (results not shown)) of the initial infection can impact the timing of the epidemic – essentially translating the epidemic trajectory in the time axis. When more infectious individuals seed an outbreak, the epidemic trajectory emerges earlier than if the initial case is less infectious than average – in which case the epidemic occurs more slowly than expected under the outbreak eigendistribution and baseline SIR models. As the infection has already occurred, the susceptibility of this (small) index infection does not play a role in ongoing transmission or the long-term epidemic trajectory given mass-action kinetics.

However, the susceptibility (and transmissibility) of individuals in the first few chains of infection

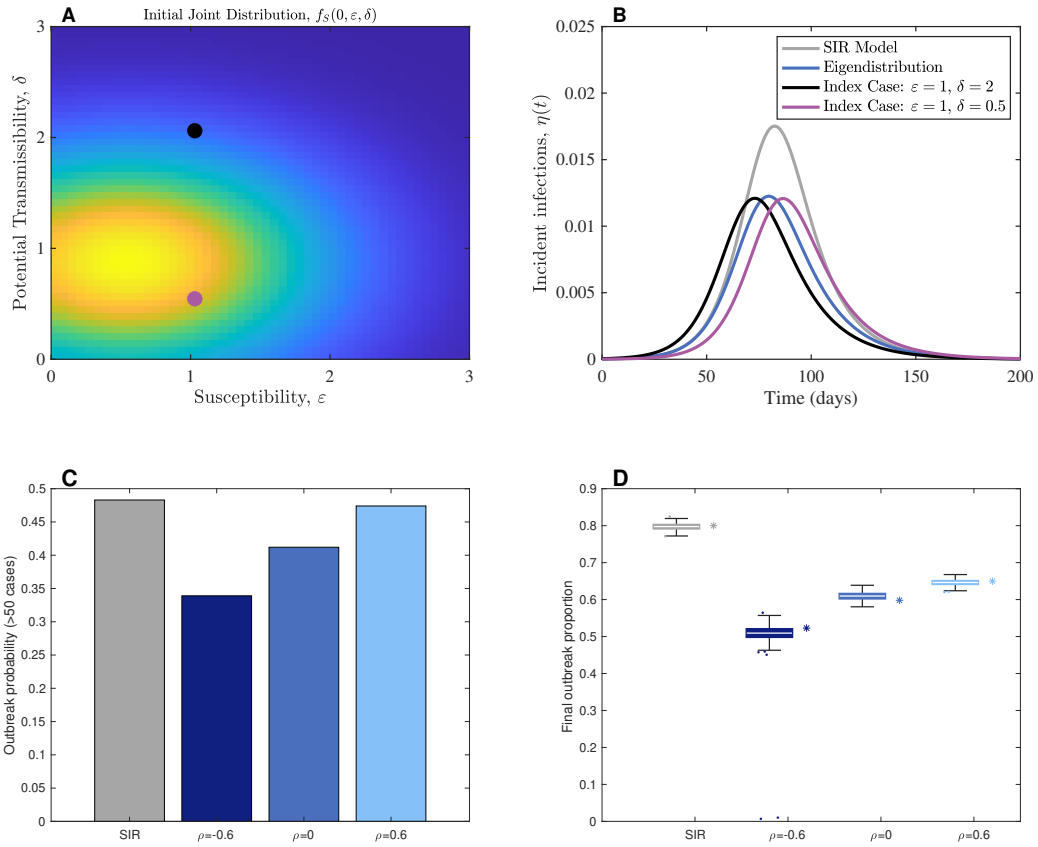

Figure 6. Sensitivity of heterogeneous models with respect to an outbreaks index case. **(A)** Two different choices for the characteristics of the initial index case index with susceptibility $\varepsilon = 1$ and transmissibility values: $\delta = 0.5$ (gray dot) and $\delta = 2$ (black dot), superimposed atop the the initial joint distribution of the uncorrelated Gaussian case. **(B)** Using the discrete model, we fix the mean susceptibility $\varepsilon = 1$ and show that varying the transmissibility of the index cases chosen in A can shift the timing of epidemic onsets and peaks. **(C)** Using stochastic simulations with a randomly chosen index case, we show the probability of an outbreak of more than 50 infections occurring for the SIR model, and for models incorporating negative correlations ($\rho = -0.60$), no correlations ($\rho = 0$) and positive correlations ($\rho = 0.60$) between susceptibility and transmissibility. **(D)** from the same stochastic ensembles as in C, variation in the final outbreak size (given that outbreaks generate more than 50 infections) is shown, outliers are shown as jittered points. Asterisk's (*) show the results from the corresponding deterministic simulations from Figure 5. Parameters: transmission rate is $\beta = 0.2$ and recovery rate is $\gamma = 0.1$. Stochastic simulations were initialized in a population of 10,000. Each stochastic ensemble consists of 1,000 trajectories.

may be important. To examine this, we adapted our model to include individual transmission events – utilising stochastic Gillespie simulations (see section E) for the baseline SIR, and the heterogeneous cases with $\rho = -0.6$, $\rho = 0$, $\rho = 0.6$ examined in Figure 5. In doing so, we show that incorporating heterogeneity can additionally alter the probability of an outbreak (here defined as more than 50 infections, see Figure 6C). While the SIR model and the uncorrelated ($\rho = 0$) model both have an initial reproduction number of $\mathcal{R}_0 = 2$, they differ in the likelihood of an outbreak occurring. For the SIR model, the outbreak probability (given m initial infections) is expected as: $p = 1 - (\frac{1}{\mathcal{R}_0})^m$ (Southall et al., 2023). With one initial index infection ($m = 1$) this supports an analytic outbreak probability of $p = 0.5$, in close agreement with the proportion of stochastic SIR model simulations in which an outbreak occurred (0.483); but further from the uncorrelated model (0.412). The

correlated models also differ in the observed proportion of outbreaks relative to the expected outbreak probability; 0.339 vs $p = 0.371$ for the $\rho = -0.6$ case, and 0.474 vs. $p = 0.5887$ for the $\rho = 0.6$ condition. Regardless of correlation, the introduction of heterogeneity lowers the expected outbreak probability relative to the SIR baseline. Utilizing a stochastic framework also allows us to assess variability in epidemic trajectories (see Figure 6D) whose average final sizes for simulations that ran to epidemic burnout (i.e., simulations which ended due to susceptible depletion, rather than fizzling out) are in good agreement with the deterministic simulations. Histograms of final outbreak size and outbreak duration for all epidemic trajectories are shown in Figure S4. Together with Figure 5 we observe that within our framework, positive correlations between susceptibility and transmissibility lead to epidemics that are more likely to occur, and are faster (with shorter duration), stronger (higher incident infections and final outbreak size) and less variable (final outbreak size IQR = 0.0112, for $\rho = 0.6$), while negative correlation outbreaks are on average less likely to occur, have longer duration and lower, but more variable final size (final outbreak size IQR = 0.0239, for $\rho = -0.6$).

3.5 The effects of correlations on epidemic progress

Next, we consider how initial correlations between susceptibility and transmissibility of the population impact the progress of the epidemic – i.e., for an epidemic identified with a particular $\mathcal{R}_0$ how might covariation in susceptibility and transmissibility impact the epidemic trajectory? To address this question, we vary the correlation coefficient, ρ, and match the exponential growth rate of incident infections by adjusting the transmission rate, β (Figure 7A). We compare across simulations the epidemic dynamics during susceptible depletion using the progress variable, $\bar{\varepsilon}(t)$, i.e., the mean susceptibility (Figure 7B). For $\bar{\varepsilon}(t_1) = 0.9$, both positive (light blue) and negative correlations (dark blue) reach this susceptibility level at a similar rate compared to without correlations (light blue). For negative correlations, the effective transmission rate increases over time, whereas for positive correlations, the effective transmission rate decreases over time (Figure 7C). At mean susceptibility, $\bar{\varepsilon}(t_1) = 0.9$, the susceptible population is depleted to about 80% of the population (Figure 7D). The marginal distributions for susceptibility are similar for different scenarios but differ somewhat due to different truncation for the different correlation coefficients (Figure 7E). The marginal distributions for transmissibility do differ at $\bar{\varepsilon}(t_1) = 0.9$: positive correlations initialize the transmissibility distribution to the right of the transmissibility distribution without correlations, whereas negative correlations initialize the transmissibility distribution to the left of the transmissibility distribution without correlations (Figure 7F). Since more susceptible individuals are infected earlier during the epidemic with positive correlations, the more susceptible individuals are also more transmissible, leading to increases in the initial speed and strength of the outbreak. With negative correlations, individuals who are more susceptible are less transmissible, leading to decreases in the initial speed and strength.

3.6 The dynamics of the susceptibility and transmissibility distributions as the epidemic progresses

To compare across different correlation cases, we examine susceptibility and transmissibility marginal distributions over time, comparing across simulations using the epidemic progress variable at values: $\bar{\varepsilon} = 1.0, 0.90, 0.80, 0.66$ (Figure 8A, middle). For different correlation coefficients, the mean susceptibility, $\bar{\varepsilon}$, decreases at different rates due to differences in the dynamics of the effective transmission rates (Figure 8A, bottom). We show the susceptibility (Figure 8B) and transmissibility distributions (Figure 8C) over the epidemic progress variable (panels going down): Without correlations ($\rho = 0$, the effective transmission rate remains constant (Figure 8A). For positive correlations ($\rho > 0$), the effective transmission rate decreases over time, whereas for negative correlations ($\rho < 0$), the effective transmission rate increases over time. Hence, in either case, the transmissibility distributions tend toward the mean transmissibility of $\lim_{t\to\infty} \bar{\delta}(t) = 1$ (Figure 8C), despite opposite tendencies in the effective transmission rate (Figure 8A, bottom panel).

From equations Equation 11 and Equation 13, the joint distribution in the infected population

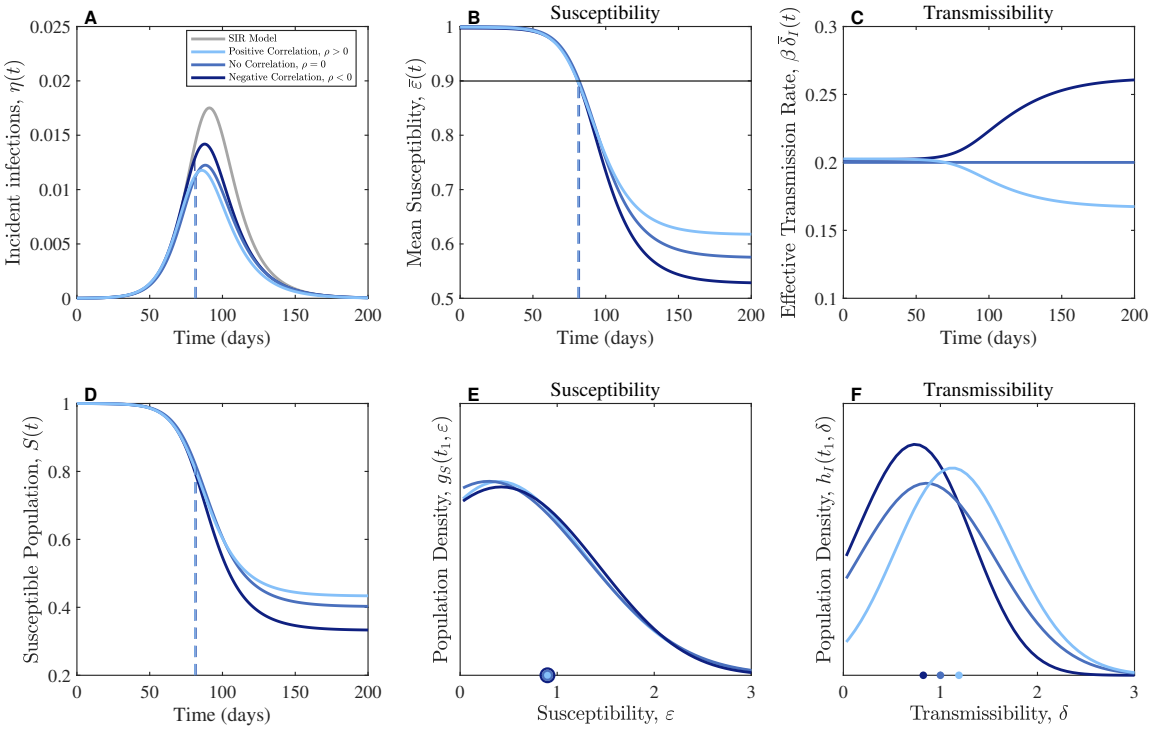

Figure 7. The effects of correlations between susceptibility and transmissibility when the exponential growth rate is matched. (A) Incident infections. **(B)** Mean susceptibility decreases over time as the susceptible population is depleted. **(C)** Without correlations, the effective transmission rate remains constant (medium blue). Positive correlations cause the transmissibility to decrease over time (light blue), whereas negative correlations cause susceptibility to increase over time (dark blue). **(D)** About 80% of the susceptible population is depleted. **(E)** Susceptibility distributions plotted at $\bar{\varepsilon}(t_1) = 0.9$. **(F)** Transmissibility distribution at time points corresponding to the progress variable, $\bar{\varepsilon}(t_1) = 0.9$. For positive (negative) correlations, the mean transmissibility is greater (less) than the mean transmissibility without correlations. Across all simulations, the recovery rate is $\gamma = 1/10$ and the basic reproduction number is $\mathcal{R}_0 = 2.0$. The transmission rates vary: $\beta = 0.254,\ 0.2,\ 0.165$ for positive correlation, no correlation, and negative correlation, respectively. The initial variance values are: $\sigma^2_\varepsilon(0) = 0.44, 0.50, 0.30$, and $\sigma^2_\delta(0) = 0.27, 0.35, 0.30$.

satisfies the partial differential equation:

$$\frac{\partial f_I(t,\varepsilon,\delta)}{\partial t} = \beta\,\bar{\delta}_I\,S\,\left(\varepsilon\,f_S(t,\varepsilon,\delta) - \bar{\varepsilon}\,f_I(t,\varepsilon,\delta)\right)\,. \tag{22}$$

Integrating over ε, the effective transmissibility distribution satisfies the partial differential equation:

$$\frac{\partial h_I(t,\delta)}{\partial t} = \beta\,\bar{\delta}_I\,S\left(\int_0^\infty \varepsilon\,f_S(t,\varepsilon,\delta)\,d\varepsilon - \bar{\varepsilon}\,h_I(t,\delta)\right)\,. \tag{23}$$

In the case of uncorrelated susceptibility and transmissibility values, $\int_0^\infty \varepsilon\,f_S(t,\varepsilon,\delta)\,d\varepsilon = \bar{\varepsilon}\,h_S(t,\delta)$, which means that the effective transmissibility distribution remains constant and equal to the potential transmissibility distribution in the susceptible population, if they are initially equal. The mean effective transmissibility remains constant, here equal to $\bar{\delta}_I = 1$ (Figure 8C; medium blue dot). For positive correlations, the mean effective transmissibility is greater than in the case without correlations (Figure 8C; light blue dot), whereas for negative correlations, the mean effective transmissibility is less than in the case without correlations (Figure 8C; dark blue dot). For positive (negative) correlations

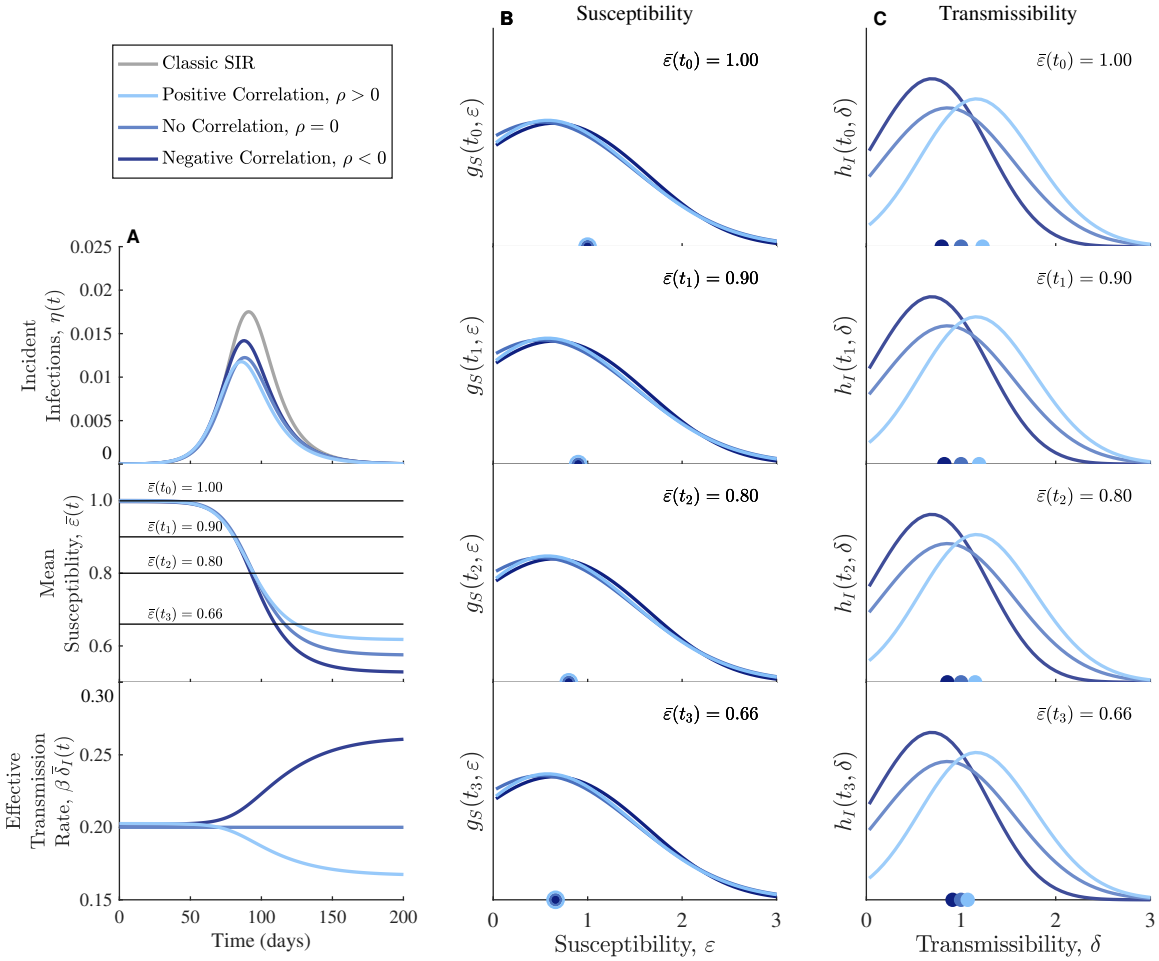

Figure 8. The effects of correlations on susceptibility and transmissibility distributions over time. (A) Population dynamics including incident infections (η), the mean susceptibility ($\bar{\varepsilon}$) (both redrawn from Figure 7A,B), and the effective transmission rate ($\beta\,\bar{\delta}_I$) . **(B)** Susceptibility distributions associated with four mean susceptibility values going down the rows: $\bar{\varepsilon} = [1.0, 0.90, 0.80, 0.66]$. **(C)** Effective transmissibility distributions at the same four time points corresponding to the mean susceptibility values. Parameter values are the same as in Figure 7.

between susceptibility and transmissibility, initial incident infections are comprised of more (less) transmissible individuals. Thus, for positive correlations, $\int_0^\infty \varepsilon\, f_S(t, \varepsilon, \delta)\, d\varepsilon > \bar{\varepsilon}\, h_I(t, \delta)$ such that $\bar{\delta}_I$ monotonically decreases toward $\bar{\delta}_I = 1$, whereas for negative correlations, $\int_0^\infty \varepsilon\, f_S(t, \varepsilon, \delta)\, d\varepsilon < \bar{\varepsilon}\, h_I(t, \delta)$ such that $\bar{\delta}_I$ monotonically increases toward $\bar{\delta}_I = 1$.

Overall, our simulations of the full PDE model (Equation 11) agree with the analysis here. In particular, correlations modify the speed of susceptible depletion such that the epidemic slows down with positive correlations and speeds up with negative correlations between susceptibility and transmissibility. Consistent with previous results on heterogeneity in susceptibility, the final outbreak sizes are all less than in the classic SIR model. In this example, the uncorrelated case leads to about 60% of the initial susceptible population becoming infected, whereas the SIR model leads to about 80% of the susceptible population becoming infected (Figure S2A).

3.7 The effects of positive correlations between susceptibility and transmissibility on the overdispersion in transmission over time

In several infectious diseases (e.g., SARS, measles) transmission is measured to be overdispersed and positively correlated with susceptibility (Lloyd-Smith et al., 2005). Here, we examine this scenario (using bivariate negative binomial distribution) with initially overdispersed transmission rates and allowing them to evolve over time in our PDE model framework. We set the initial joint distribution of susceptibility and transmissibility following a positive correlated ($\rho = 0.6$) bivariate negative binomial distribution with overdispersion in transmissibility, but not susceptibility. Details regarding this initial joint distribution are given in Appendix C where the dispersion parameter for susceptibility is: $\xi_\varepsilon = 50$, and transmissibility is overdispersed with: $\xi_\delta = 0.05$, which corresponds to estimates for Monkeypox (Lloyd-Smith et al., 2005). As in the prior models with heterogeneity we show that cumulative infections are much lower relative to the classic SIR model (Figure 9A, top). Similar to Figure 8, we use the mean susceptibility as the epidemic progress variable and show the marginal distributions of susceptibility and transmissilibity for: $\bar{\varepsilon} = 1$, $\bar{\varepsilon} = 0.70$, $\bar{\varepsilon} = 0.50$, and $\bar{\varepsilon} = 0.30$ (Figure 9B,C). We see similar trends between the uncorrelated case ($\rho = 0$) and the positively correlated case ($\rho > 0$). With positive correlations the overall effective transmissibility decreases over the course of the epidemic relative to that without correlations, which remains constant (Figure 9A, bottom). However, the underlying mean susceptibility (Figure 9A, middle) and transmissibility (Figure 9C, light blue dots on the axes) are greater on average over the course of the epidemic (i.e., the transmission rate is rescaled to match the basic reproduction number).

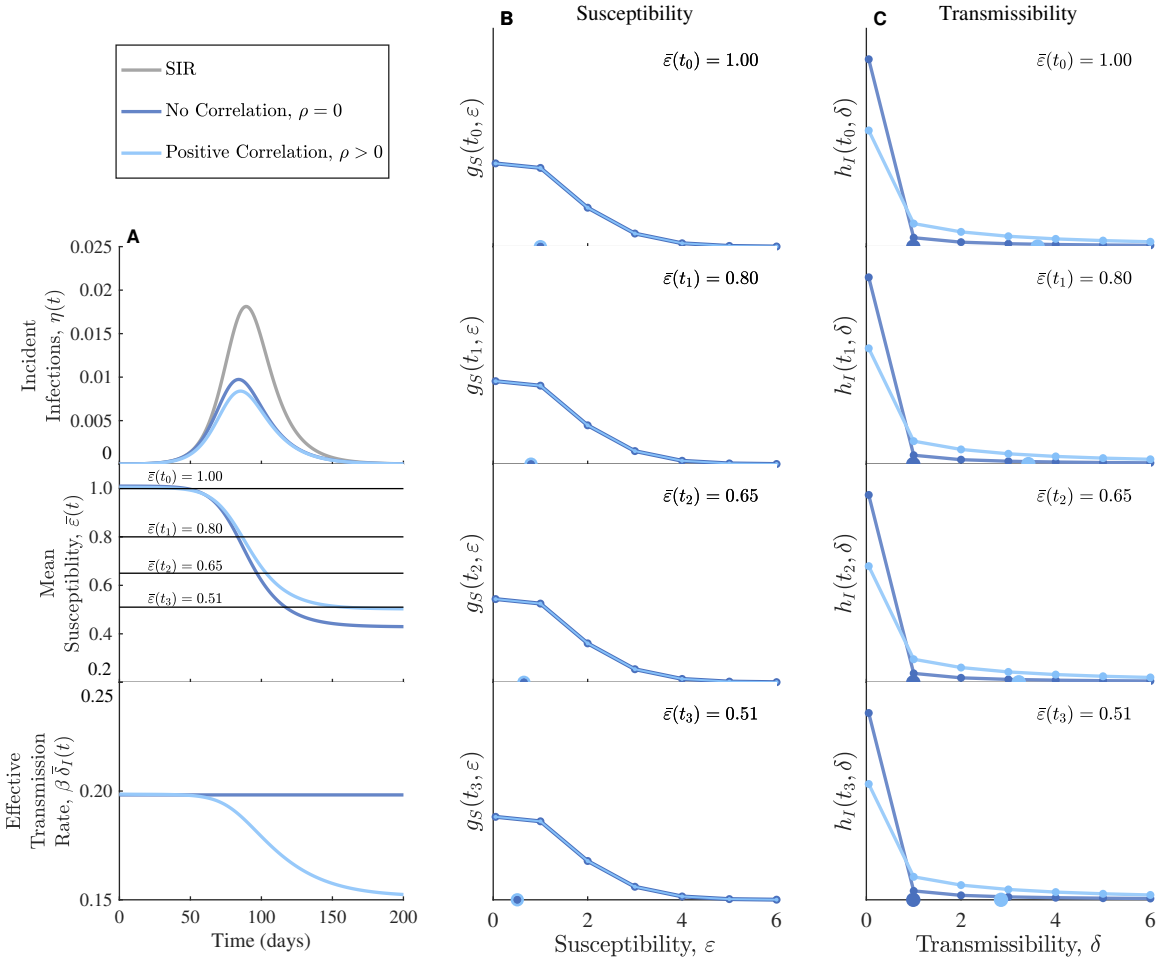

Figure 9. The effects of positive correlations on dispersion over time. (A) Population dynamics including: incident infections, initial joint susceptibility and potential transmissibility, and progression for mean susceptibility and effective transmissibility over time. **(B)** Susceptibility distributions shown at four mean susceptibility, values going down the rows: $\bar{\varepsilon} = [1.0, 0.8, 0.65, 0.51]$. **(C)** Effective transmissibility distributions at the four time points corresponding to the susceptibility values. Parameter values: $\gamma = 0.1$, $\mathcal{R}_0 = 2$. Transmissibility has a dispersion parameter: $\xi_\delta = 0.05$, and susceptibility dispersion parameter $\xi_\varepsilon = 50$. Without correlations ($\rho = 0$), $\beta = 0.2$. For the positively correlated case ($\rho = 0.6$), $\beta = 0.0548$ so that the exponential growth rate is matched. Corresponding coefficients of variation (squared) are shown in Figure S3.

4 Discussion

We developed an epidemic model framework incorporating population-level covariation in both individual susceptibility and transmissibility. Our work investigates how susceptibility and transmissibility distributions are "sculpted" over the course of an epidemic, and how correlated variation may effect population-level dynamical outcomes. We find that initial gamma and Gaussian distributions are eigendistributions of the force of infection; and that when susceptibility and transmissibility are uncorrelated this model can be reduced to a model in which average transmissibility is fixed and only susceptibility varies. Moving to exploring covariation, we identified a relation between $\mathcal{R}_0$ and the correlation of initial potential transmissibility and susceptibility. Keeping β and γ constant, we found that when susceptibility and transmissibility are correlated (anticorrelated), then $\mathcal{R}_0$ increases

(decreases), epidemics initially grow faster (slower) and are more (less) likely to become outbreaks, and infect more (fewer) individuals. However, if instead $\mathcal{R}_0$ is kept constant, we find models with covariation share the same initial epidemic speed, but differ in outcome. In order to keep $\mathcal{R}_0$ fixed, and introducing negative correlations between susceptibility and transmissibility necessitates increasing the average transmission rate β (or decreasing the average recovery rate γ), leading to larger epidemics and additionally leading to an increase in the effective transmission rate over time, as individuals who are both highly susceptible and less transmissible are sculpted into the epidemic earlier on, leaving behind a less susceptible, but more transmissible population. Finally, we utilised our framework to assess the effects of overdispersed transmission on epidemic sculpting. Including positive correlations in addition to overdispersed transmission may counterintuitively reduce the effective transmission over time. [**SJB:** *double-check this lines up with our results section*]

This approach comes with caveats, insofar as we focus on inherent differences in individual susceptibility and transmissibility in a well-mixed population without vital dynamics and without the potential for reinfections. Going beyond inherent differences, recent work has highlighted that individual-level susceptibility and transmissibility can be associated with human behavior via risk-perceptive decision making. Importantly, coupling informed human behaviour with disease dynamics can lead to conditions where dynamic changes in susceptibility (via changing behaviors) can explain epidemic peaks, oscillations, and shoulder behaviors (Weitz et al., 2020; Berestycki et al., 2023). The current model does not allow individual susceptibility or transmissibility to change in time, unlike Weitz et al., 2020 (while neglecting heterogeneity) and Berestycki et al., 2023 (while neglecting variability in transmissibility). Joint dynamic changes in the underlying distributional landscape of susceptibility and transmissibility are likely to enrich the potential dynamic behaviour. Incorporating reinfection and vital dynamics might also enrich the observed dynamics and could allow one to probe differences in heritability of epidemiologically relevant life-history traits. While epidemic burnout is expected in well-mixed SIR models, even with vital dynamics (Parsons et al., 2024), population contact structure is also a highly relevant driver of disease dynamics (Keeling & Eames, 2005; Bansal et al., 2007; Funk et al., 2010). Future extensions might consider additional dynamical effects caused by incorporating additional parameter covariation with recovery rates, heterogeneity in vaccination (Saad-Roy et al., 2024), or with population contact structure. Additionally, further investigation of how susceptibility and transmissibility distributions connect to other distributions of interest, such as the secondary attack rate (Anderson et al., 2023), is warranted.

There are also important questions related to parameter inference and outbreak control. As we and others have shown, incorporating individual-level variation provides departures from baseline SIR dynamics (Novozhilov, 2008; Novozhilov, 2012; Karev & Novozhilov, 2019; Britton et al., 2020; Rose et al., 2021; Gomes et al., 2022; Anderson et al., 2023). In early outbreaks $\mathcal{R}_0$ is one of the first parameters epidemiologists attempt to infer, yet our framing suggests $\mathcal{R}_0$ might be entangled with covariation in susceptibility and transmissibility. For an identified value of $\mathcal{R}_0$, we might expect different epidemic trajectories depending on the degree of covariation in the population. On the other hand, if $\mathcal{R}_0$ is identified via average estimations of β and γ, the degree of co-variation in the population may lead to mischaracterization of the diseases $\mathcal{R}_0$. In well-mixed populations we expect epidemics will rapidly move to sculpting from the underlying eigendistributions, but these may be difficult to identify in circumstances where transmission pathways are more heterogeneous. Utilizing new inference approaches and data types will be required to identify the degree of covariation between relevant disease parameters e.g., (Kuylen et al., 2022; Anderson et al., 2023; Tran-Kiem & Bedford, 2024; Tuschhoff & Kennedy, 2024). Beyond inference of $\mathcal{R}_0$ as an early indicator of implementing control measures, there may be additional ramifications if susceptibility or transmissibility covary with infection severity. With a public health goal of minimizing severe outcomes across populations, then if severity is correlated with susceptibility and/or anti-correlated with transmissibility then stronger control measures may be required.

In closing, our work shows how individual-level heterogeneity scales up to population-level epidemiological consequences. In particular, we demonstrate the importance of considering both variation and covariation between susceptibility and transmissibility. Identifying dynamical hallmarks

of covariation, and quantifying how multi-dimensional (dynamical) covariation drives population dynamics offer important future avenues to explore. Such frameworks and understanding go beyond the epidemiological context within which our current research is embedded.

CRediT authorship contribution statement

Jeremy D. Harris: Conceptualization, Formal analysis, Investigation, Software, Supervision, Visualization, Writing – original draft, Writing – review & editing. **Esther Gallmeier:** Conceptualization, Formal analysis, Investigation, Software, Visualization, Writing – review & editing. **Stephen J. Beckett:** Investigation, Software, Validation, Visualization, Writing – original draft, Writing – review & editing. **Joshua S. Weitz:** Conceptualization, Funding acquisition, Project administration, Writing – review & editing.

Declaration of competing interest

Author Joshua Weitz is a Co-Chief Editor of the Journal of Theoretical Biology. This article was reviewed and handled by an independent editor. Dr. Weitz was not involved in the editorial decision of the submission. The authors declare that they have no other known competing financial interests or personal relationships that could have appeared to influence the work reported in this paper.

Acknowledgements

This work was supported in part by a grant from the Simons Foundation (no. 930382 [**SJB:** *Joshua: please can you double-check this is correct for the Math Physical Sci award? It is not listed as such in what I can see.*]) and support from the Charities in Aid Foundation, the Marier Cunningham Foundation, and the Chaires Blaise Pascal program of the Île-de-France region (Blaise Pascal Institute Chair of Excellence awarded to JSW). We thank Tapan Goel for constructive feedback.

Code availability

MATLAB (version 2023b and 2024a) code for the analysis performed in this manuscript is available at https://github.com/Jeremy-D-Harris/SIR_heterogeneity_project and is archived on Zenodo (Harris et al., 2024).

Supplemental Material

Supplemental Figures

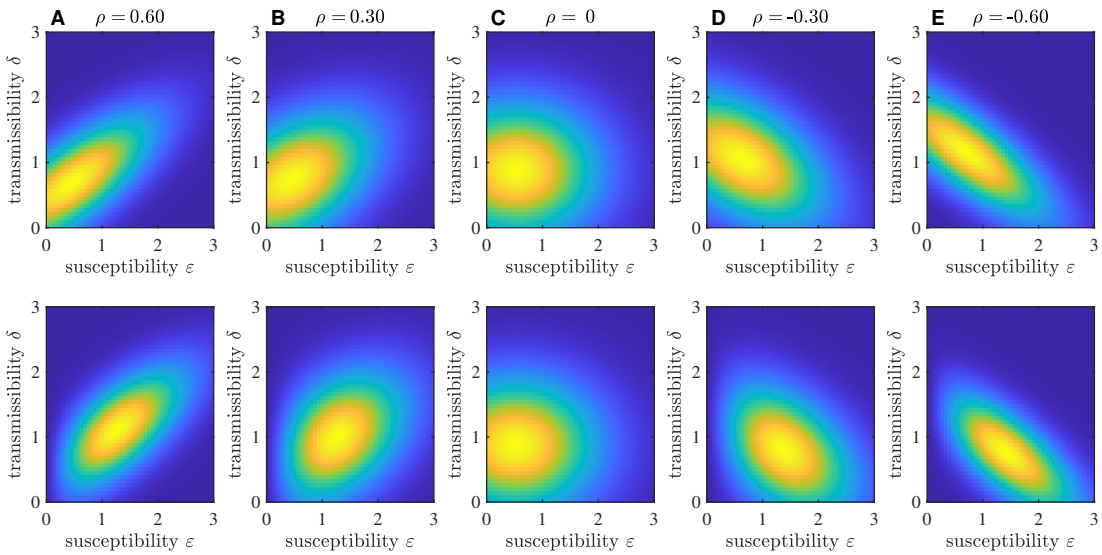

Figure S1. Initial Gaussian Joint Distributions in S (top) and I (bottom). Corresponding to simulations in Figure 5, where the joint distribution in I arises from the eigendistribution: (**A**) $\rho = -0.6$, (**B**) $\rho = -0.3$, (**C**) $\rho = 0$, (**D**) $\rho = 0.3$, (**E**) $\rho = 0.6$.

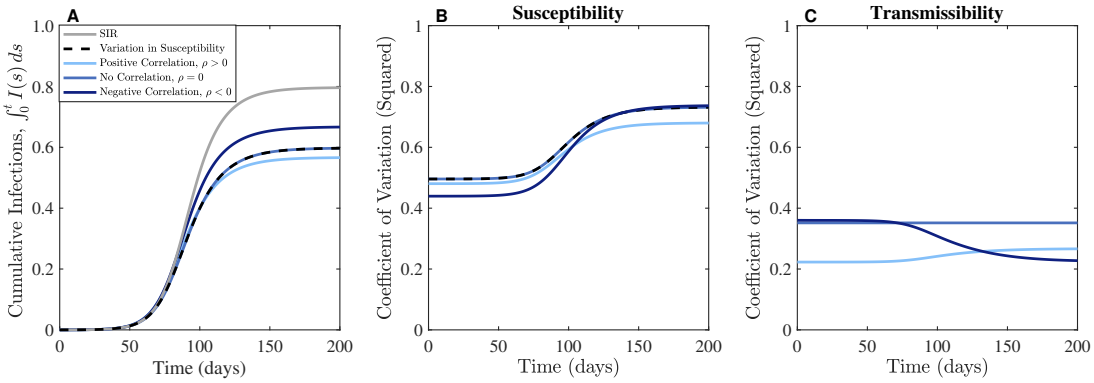

Figure S2. The effects of correlations on cumulative infections and the coefficients of variation. (**A**) Cumulative infections showing different final outbreak sizes for different correlations between susceptibility and transmissibility. Parameter values are the same as in Figure 7 and Figure 8. The coefficients of variation (squared) for susceptibility (**B**) and transmissibility (**C**).

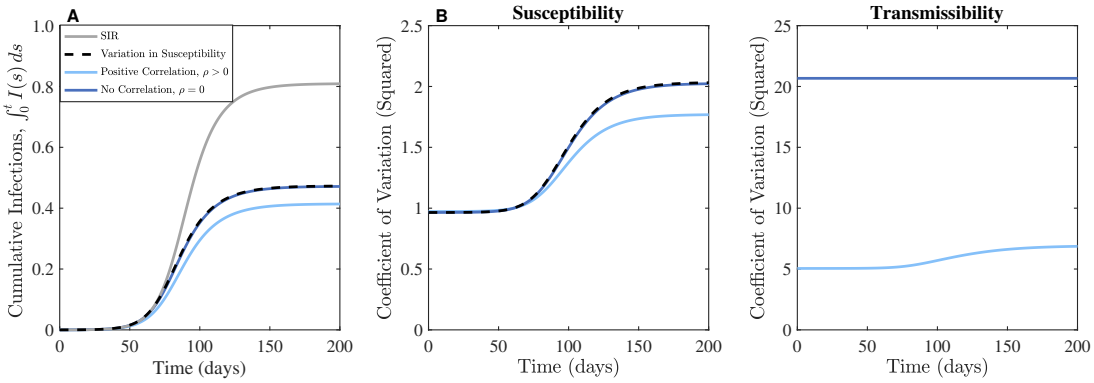

Figure S3. The effects of overdispersed transmission and positive correlations on cumulative infections and the coefficients of variation. (**A**) Cumulative infections showing different final outbreak sizes for different correlations between susceptibility and transmissibility. Parameter values are the same as in Figure 9. The coefficients of variation (squared) for susceptibility (**B**) and transmissibility (**C**).

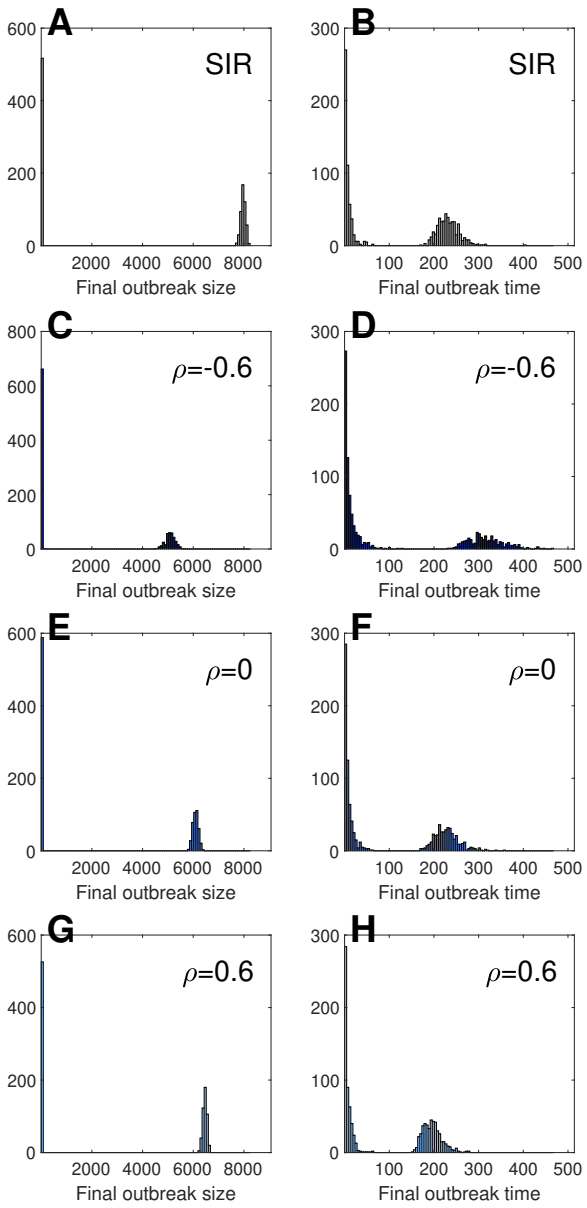

Figure S4. Stochastic variability in epidemic outbreak size and duration. Count histograms from the four ensembles of 1,000 simulations of epidemic trajectories shown in Figure 6C,D. Final outbreak size **(A)** and duration (days) **(B)** for the SIR model, where 51.7% of simulations generated $\leq$50 infections. Final outbreak size **(C)** and duration (days) **(D)** for the model with negative correlation between susceptibility and potential transmissibility ($\rho = -0.6$), where 66.1% of simulations generated $\leq$50 infections. Final outbreak size **(E)** and duration (days) **(F)** for the model with no correlation between susceptibility and potential transmissibility ($\rho = 0$), where 58.8% of simulations generated $\leq$50 infections. Final outbreak size **(G)** and duration (days) **(H)** for the model with positive correlation between susceptibility and potential transmissibility ($\rho = 0.6$), where 52.6% of simulations generated $\leq$50 infections. Parameters: transmission rate is $\beta = 0.2$ and recovery rate is $\gamma = 0.1$. Stochastic simulations were initialized in a population of 10,000.

References

Kermack, W. O., & McKendrick, A. G. (1927). A contribution to the mathematical theory of epidemics. *Proceedings of the Royal Society of London. Series A, Containing papers of a Mathematical and Physical Character*, *115*(772), 700–721. https://doi.org/10.1098/rspa.1927.0118

Gart, J. J. (1972). The statistical analysis of chain-binomial epidemic models with several kinds of susceptibles. *Biometrics*, *28*, 921–930. https://doi.org/10.2307/2528629

Gillespie, D. T. (1976). A general method for numerically simulating the stochastic time evolution of coupled chemical reactions. *Journal of computational physics*, *22*(4), 403–434. https://doi.org/10.1016/0021-9991(76)90041-3

Gillespie, D. T. (1977). Exact stochastic simulation of coupled chemical reactions. *The Journal of Physical Chemistry*, *81*(25), 2340–2361. https://doi.org/10.1021/j100540a008

Dormand, J. R., & Prince, P. J. (1980). A family of embedded Runge-Kutta formulae. *Journal of computational and applied mathematics*, *6*(1), 19–26. https://doi.org/10.1016/0771-050X(80)90013-3

Ball, F. (1985). Deterministic and stochastic epidemics with several kinds of susceptibles. *Advances in applied probability*, *17*(1), 1–22. https://doi.org/10.2307/1427049

Dushoff, J., & Levin, S. (1995). The effects of population heterogeneity on disease invasion. *Mathematical biosciences*, *128*(1-2), 25–40. https://doi.org/10.1016/0025-5564(94)00065-8

Dwyer, G., Elkinton, J. S., & Buonaccorsi, J. P. (1997). Host heterogeneity in susceptibility and disease dynamics: Tests of a mathematical model. *The American Naturalist*, *150*(6), 685–707. https://doi.org/10.1086/286089

Shampine, L. F., & Reichelt, M. W. (1997). The MATLAB ODE suite. *SIAM journal on scientific computing*, *18*(1), 1–22. https://doi.org/10.1137/S1064827594276424

Coutinho, F., Massad, E., Lopez, L., Burattini, M., Struchiner, C., & Azevedo-Neto, R. (1999). Modelling heterogeneities in individual frailties in epidemic models. *Mathematical and computer modelling*, *30*(1-2), 97–115. https://doi.org/10.1016/S0895-7177(99)00119-3

Dwyer, G., Dushoff, J., Elkinton, J. S., & Levin, S. A. (2000). Pathogen-driven outbreaks in forest defoliators revisited: Building models from experimental data. *The American Naturalist*, *156*(2), 105–120. https://doi.org/10.1086/303379

Keeling, M. J., & Eames, K. T. (2005). Networks and epidemic models. *Journal of the Royal Society Interface*, *2*(4), 295–307. https://doi.org/10.1098/rsif.2005.0051

Lloyd-Smith, J. O., Schreiber, S. J., Kopp, P. E., & Getz, W. M. (2005). Superspreading and the effect of individual variation on disease emergence. *Nature*, *438*(7066), 355–359. https://doi.org/10.1038/nature04153

Bansal, S., Grenfell, B. T., & Meyers, L. A. (2007). When individual behaviour matters: Homogeneous and network models in epidemiology. *Journal of The Royal Society Interface*, *4*(16), 879–891. https://doi.org/10.1098/rsif.2007.1100

Novozhilov, A. S. (2008). On the spread of epidemics in a closed heterogeneous population. *Mathematical Biosciences*, *215*(2), 177–185. https://doi.org/10.1016/j.mbs.2008.07.010

Famoye, F. (2010). On the bivariate negative binomial regression model. *Journal of Applied Statistics*, *37*(6), 969–981. https://doi.org/10.1080/02664760902984618

Funk, S., Salathé, M., & Jansen, V. A. (2010). Modelling the influence of human behaviour on the spread of infectious diseases: A review. *Journal of the Royal Society Interface*, *7*(50), 1247–1256. https://doi.org/10.1098/rsif.2010.0142

Novozhilov, A. S. (2012). Epidemiological models with parametric heterogeneity: Deterministic theory for closed populations. *Mathematical Modelling of Natural Phenomena*, *7*(3), 147–167. https://doi.org/10.1051/mmnp/20127310

Karev, G. P., & Novozhilov, A. S. (2019). How trait distributions evolve in populations with parametric heterogeneity. *Mathematical Biosciences*, *315*, 108235. https://doi.org/10.1016/j.mbs.2019.108235

Britton, T., Ball, F., & Trapman, P. (2020). A mathematical model reveals the influence of population heterogeneity on herd immunity to SARS-CoV-2. *Science*, *369*(6505), 846–849. https://doi.org/10.1126/science.abc6810

Davies, N. G., Klepac, P., Liu, Y., Prem, K., Jit, M., & Eggo, R. M. (2020). Age-dependent effects in the transmission and control of COVID-19 epidemics. *Nature medicine*, *26*(8), 1205–1211. https://doi.org/10.1038/s41591-020-0962-9

Weitz, J. S., Park, S. W., Eksin, C., & Dushoff, J. (2020). Awareness-driven behavior changes can shift the shape of epidemics away from peaks and toward plateaus, shoulders, and oscillations. *Proceedings of the National Academy of Sciences*, *117*(51), 32764–32771. https://doi.org/10.1073/pnas.2009911117

Zhang, J., Litvinova, M., Liang, Y., Wang, Y., Wang, W., Zhao, S., Wu, Q., Merler, S., Viboud, C., Vespignani, A., et al. (2020). Changes in contact patterns shape the dynamics of the COVID-19 outbreak in China. *Science*, *368*(6498), 1481–1486. https://doi.org/10.1126/science.abb8001

Rose, C., Medford, A. J., Goldsmith, C. F., Vegge, T., Weitz, J. S., & Peterson, A. A. (2021). Heterogeneity in susceptibility dictates the order of epidemic models. *Journal of Theoretical Biology*, *528*, 110839. https://doi.org/10.1016/j.jtbi.2021.110839

Gomes, M. G. M., Ferreira, M. U., Corder, R. M., King, J. G., Souto-Maior, C., Penha-Gonçalves, C., Gonçalves, G., Chikina, M., Pegden, W., & Aguas, R. (2022). Individual variation in susceptibility or exposure to SARS-CoV-2 lowers the herd immunity threshold. *Journal of Theoretical Biology*, 111063. https://doi.org/10.1016/j.jtbi.2022.111063

Kuylen, E. J., Torneri, A., Willem, L., Libin, P. J., Abrams, S., Coletti, P., Franco, N., Verelst, F., Beutels, P., Liesenborgs, J., & Hens, N. (2022). Different forms of superspreading lead to different outcomes: Heterogeneity in infectiousness and contact behavior relevant for the case of SARS-CoV-2. *PLoS Computational Biology*, *18*(8), e1009980. https://doi.org/10.1371/journal.pcbi.1009980

Lovell-Read, F. A., Shen, S., & Thompson, R. N. (2022). Estimating local outbreak risks and the effects of non-pharmaceutical interventions in age-structured populations: SARS-CoV-2 as a case study. *Journal of Theoretical Biology*, *535*, 110983. https://doi.org/10.1016/j.jtbi.2021.110983

Allard, A., Moore, C., Scarpino, S. V., Althouse, B. M., & Hébert-Dufresne, L. (2023). The role of directionality, heterogeneity, and correlations in epidemic risk and spread. *SIAM Review*, *65*(2), 471–492. https://doi.org/10.1137/20m1383811

Anderson, T. L., Nande, A., Merenstein, C., Raynor, B., Oommen, A., Kelly, B. J., Levy, M. Z., & Hill, A. L. (2023). Quantifying individual-level heterogeneity in infectiousness and susceptibility through household studies. *Epidemics*, *44*, 100710. https://doi.org/10.1016/j.epidem.2023.100710

Berestycki, H., Desjardins, B., Weitz, J. S., & Oury, J.-M. (2023). Epidemic modeling with heterogeneity and social diffusion. *Journal of Mathematical Biology*, *86*(4), 60. https://doi.org/10.1007/s00285-022-01861-w

Meehan, M. T., Hughes, A., Ragonnet, R. R., Adekunle, A. I., Trauer, J. M., Jayasundara, P., McBryde, E. S., & Henderson, A. S. (2023). Replicating superspreader dynamics with compartmental models. *Scientific Reports*, *13*(1), 15319. https://doi.org/10.1038/s41598-023-42567-3

Murayama, H., Pearson, C. A. B., Abbott, S., Miura, F., Jung, S.-m., Fearon, E., Funk, S., & Endo, A. (2023). Accumulation of immunity in heavy-tailed sexual contact networks shapes Mpox outbreak sizes. *The Journal of Infectious Diseases*, *229*(1), 59–63. https://doi.org/10.1093/infdis/jiad254

Southall, E., Ogi-Gittins, Z., Kaye, A., Hart, W., Lovell-Read, F., & Thompson, R. (2023). A practical guide to mathematical methods for estimating infectious disease outbreak risks. *Journal of Theoretical Biology*, *562*, 111417. https://doi.org/10.1016/j.jtbi.2023.111417

Harris, J. D., Gallmeier, E., Beckett, S. J., & Weitz, J. S. (2024). Code for: [**SJB:** *fill this in*]XXXXXXXXXXXXX [Zenodo, doi: 10.5281/zenodo.XXX]. https://doi.org/10.5281/zenodo.XXX

Parsons, T. L., Bolker, B. M., Dushoff, J., & Earn, D. J. (2024). The probability of epidemic burnout in the stochastic SIR model with vital dynamics. *Proceedings of the National Academy of Sciences*, *121*(5), e2313708120. https://doi.org/10.1073/pnas.2313708120

Saad-Roy, C. M., Morris, S. E., Boots, M., Baker, R. E., Lewis, B. L., Farrar, J., Marathe, M. V., Graham, A. L., Levin, S. A., Wagner, C. E., Metcalf, C. J. E., & Grenfell, B. T. (2024). Impact of waning immunity against SARS-CoV-2 severity exacerbated by vaccine hesitancy. *PLOS Computational Biology*, *20*(8), e1012211. https://doi.org/10.1371/journal.pcbi.1012211

Tran-Kiem, C., & Bedford, T. (2024). Estimating the reproduction number and transmission heterogeneity from the size distribution of clusters of identical pathogen sequences. *Proceedings of the National Academy of Sciences*, *121*(15), e2305299121. https://doi.org/10.1073/pnas.2305299121

Tuschhoff, B. M., & Kennedy, D. A. (2024). Detecting and quantifying heterogeneity in susceptibility using contact tracing data. *PLOS Computational Biology*, *20*(7), e1012310. https://doi.org/10.1371/journal.pcbi.1012310

A Derivation of susceptibility and transmissibility from discrete model variables

First, we write the susceptible (S) infected (I), and recovered (R) populations in terms of discrete model variables: $S_{i,j}$, $I_{i,j}$, and $R_{i,j}$, where i and j are indices for the discrete susceptibility value, ε_i, and transmissibility value, δ_j. Then the force of infection for the susceptible population with susceptibility level ε_i is

$$\lambda_i(t) = \beta\,\varepsilon_i \left(\sum_k \sum_j \delta_j\, I_{k,j}(t)\, d\delta_j\, d\varepsilon_k \right) = \beta\, I(t)\, \bar{\delta}_I(t)\, \varepsilon_i\,, \tag{A1}$$

where $I(t)$ is the total infected population and $\bar{\delta}_I(t)$ is the mean of the effective transmissibility distribution. We can write the discrete model equations as

$$\begin{aligned} \dot{S}_{i,j}(t) &= -\lambda_i(t)\, S_{i,j}(t) \\ \dot{I}_{i,j}(t) &= \lambda_i(t)\, S_{i,j}(t) - \gamma\, I_{i,j}(t) \\ \dot{R}_{i,j}(t) &= \gamma\, I_{i,j}(t)\ , \end{aligned} \tag{A2}$$

where γ is the recovery rate for infected individuals. This discrete model forms the basis of the continuous model equations given in Equation 11 with the connection between discrete and continuous model variables given as follows: $S_{i,j} = S(t, \varepsilon_i, \delta_j)$, $I_{i,j} = I(t, \varepsilon_i, \delta_j)$, and $R_{i,j} = R(t, \varepsilon_i, \delta_j)$. We can calculate the the total incidence:

$$\begin{aligned} \eta(t) &= \sum_i \sum_j \lambda_i(t)\, S_{i,j}(t)\, d\delta_j\, d\varepsilon_i \\ &= \beta\, I(t)\, \bar{\delta}_I(t) \sum_i \sum_j \varepsilon_i S_{i,j}(t)\, d\delta_j\, d\varepsilon_i \\ &= \beta\, I(t)\, \bar{\delta}_I(t)\, \bar{\varepsilon}(t)\, S(t)\,. \end{aligned}$$

Next, we derive differential equations for $\dot{\bar{\varepsilon}}(t)$, $\dot{\bar{\delta}}_S(t)$, and $\dot{\bar{\delta}}_I(t)$ found in Equation 13 in terms of discrete model variables. For $\dot{\bar{\varepsilon}}(t)$, we examine the time derivative of total susceptibility,

$$\dot{E}_S := \sum_j \sum_i \varepsilon_i\, \dot{S}_{i,j} = -\beta\, I\, \bar{\delta}_I \left(\sum_j \sum_i \varepsilon_i^2\, S_{i,j} \right)\,.$$

Note that $\sum_j \sum_i \varepsilon_i^2 S_{i,j} = \bar{\varepsilon}^2 + \sigma_\varepsilon^2$. On the other hand, $\dot{E}_S = \dot{\bar{\varepsilon}}\, S + \bar{\varepsilon}\, \dot{S} = \dot{\bar{\varepsilon}}\, S - \bar{\varepsilon}\, \eta$. Hence,

$$\begin{aligned} \dot{\bar{\varepsilon}}\, S &= -\beta \bar{\delta}_I I(\bar{\varepsilon}^2 + \sigma_\varepsilon^2) S + \bar{\varepsilon}\, \eta \\ &= -\beta \bar{\delta}_I I(\bar{\varepsilon}^2 + \sigma_\varepsilon^2) S + \bar{\varepsilon}\, \left(\beta\, I\, \bar{\delta}_I\, \bar{\varepsilon}\, S \right) \\ &= -\beta\, \bar{\delta}_I I\, \sigma_\varepsilon^2\, S\,, \end{aligned}$$

which leads to

$$\dot{\bar{\varepsilon}} = -\beta\, \bar{\delta}_I\, I\, \sigma_\varepsilon^2\ . \tag{A3}$$

For $\dot{\bar{\delta}}_S$, we examine the time derivative of the total potential transmissibility in the susceptible population,

$$\dot{F}_S(t) := \sum \sum \delta_j \dot{S}_{i,j} = -\beta \bar{\delta}_I I \left(\sum \sum \delta_j \varepsilon_i S_{i,j} \right) = -\beta\, \bar{\delta}_I\, I\, \bar{M}_S\, S\,.$$

Here, $\bar{M}_S(t) = \mathrm{cov}(\varepsilon, \delta) + \bar{\varepsilon}\, \bar{\delta}_S$ is the mean of the joint distribution of the susceptible population, where $\mathrm{cov}(\varepsilon, \delta)$ is the covariance between susceptibility and transmissibility in the susceptible population.

On the other hand, $\dot{F}_S = \dot{\bar{\delta}}_S\, S + \bar{\delta}_S\, \dot{S} = \dot{\bar{\delta}}_S\, S - \bar{\delta}_S\, \eta$. Hence,

$$\begin{aligned}\dot{\bar{\delta}}_S\, S &= -\beta\, \bar{\delta}_I\, I\, \bar{M}_S\, S + \bar{\delta}_S\, \eta \\ &= -\beta\, \bar{\delta}_I\, I\, \bar{M}_S\, S + \bar{\delta}_S\, \beta\, I\, \bar{\delta}_I\, \bar{\varepsilon}\, S \\ &= -\beta\, \bar{\delta}_I\, I\, \left(\bar{M}_S\, - \bar{\delta}_S\, \bar{\varepsilon}\right)\, S\,,\end{aligned}$$

so that

$$\dot{\bar{\delta}}_S = -\beta\, \bar{\delta}_I\, I\, \left(\bar{M}_S\, - \bar{\delta}_S\, \bar{\varepsilon}\right)\,. \tag{A4}$$

For $\dot{\delta}_I$, we examine the time derivative the total effective transmissibility in the infected population,

$$\dot{F}_I = \sum\sum \delta_j \dot{I}_{i,j} = \beta\, \bar{\delta}_I I \left(\sum\sum \delta_j \varepsilon_i S_{i,j}\right) - \gamma\, \bar{\delta}_I I = \beta\, \bar{\delta}_I I \bar{M}_S - \gamma\, \bar{\delta}_I I\,.$$

On the other hand, $\dot{F}_I = \dot{\bar{\delta}}_I I + \bar{\delta}_I \dot{I} = \dot{\bar{\delta}}_I I + \bar{\delta}_I(\eta - \gamma\, I)$. Equating sides and simplifying, we obtain

$$\dot{\bar{\delta}}_I = \beta \bar{\delta}_I \left(\bar{M}_S - \bar{\delta}_I\, \bar{\varepsilon}\right) S\,. \tag{A5}$$

B Derivation of Equation 19

[**SJB:** *new title?*] We derive the partial differential equation that describes the evolution of the susceptible population density $f_S(t, \varepsilon, \delta)$ with intrinsic susceptibility ε and intrinsic transmissibility δ. Rearranging the definition of $f_S(t, \varepsilon, \delta)$ from Equation 1 and taking the partial derivative with respect to time, we obtain

$$\frac{\partial \left(S(t) f_S(t, \varepsilon, \delta)\right)}{\partial t} = \frac{\partial S(t, \varepsilon, \delta)}{\partial t}. \tag{B6}$$

Expansion of the left-hand side through the product rule and the use of Equation 11 give us

$$\dot{S}(t) f_S(t, \varepsilon, \delta) + S(t) \frac{\partial f_S(t, \varepsilon, \delta)}{\partial t} = -\lambda(t, \varepsilon) S(t, \varepsilon, \delta). \tag{B7}$$

Recalling the definition of $\dot{S}(t)$ described in Equation 13, and expanding λ from Equation 10, we obtain

$$-\beta I \bar{\delta}_I \bar{\varepsilon} S(t) f_S(t, \varepsilon, \delta) + S(t) \frac{\partial f_S(t, \varepsilon, \delta)}{\partial t} = -\beta I \bar{\delta}_I \varepsilon S(t) f_S(t, \varepsilon, \delta), \tag{B8}$$

which after rearranging yields the partial differential equation in Equation 19.

C Initial joint distributions of susceptibility and transmissibility

To incorporate variation in both susceptibility and transmissibility we use bivariate distributions to initialize our epidemiological models. We do so by first creating the initial joint bivariate distribution in S, using a built-in function from the Statistics and Machine Learning Toolbox (MATLAB version 2023b and 2024a) for the specific probability distributions used. Without correlations between susceptibility and transmissibility, the initial joint distributions in f_I and f_R are set equal to that in f_S. When correlations are introduced, the initial conditions of f_I and f_R are approximated via the attracting eigendistribution during the exponential growth phase of the epidemic from a preliminary simulation. In this work, we consider three types of bivariate distributions: gamma, truncated Gaussian, and negative binomial.

We first consider independent gamma distributions for the initial joint distribution for susceptibility (ε) and transmissibility (δ). However, these independent gamma distributions do not allow for

covariation in ε and δ. Hence, we consider the bivariate Gaussian distribution with 2×2 covariance matrix, allowing us to compare the effects of increasing covariation on epidemic dynamics. We increase the initial variance in susceptibility ($\sigma_\varepsilon(0)$) and transmissibility ($\sigma_\delta(0)$) to better see the effects of covariation. In doing so, the bivariate Gaussian Distributions are truncated, because their support lies on the whole real plane $\mathbb{R}^2$. We ensure that mean values are set with $\bar{\varepsilon}(0) = \bar{\delta}_S(0) = 1$ and adjust variances to match the specified correlation coefficient. In practice, truncation of distributions with high variance in susceptibility and/or transmissibility can be hard to match with large (anti)correlations. In our work, we restrict analysis to correlations between -0.6 and 0.6.

Finally, to examine epidemics with initially overdispersed transmission rates, we initialize the joint distribution using a bivariate negative binomial with dispersion parameter (ξ) and correlation coefficient (ρ) (Famoye, 2010). When $\xi < 1$ the distribution is overdispersed, with $\xi = 1$ corresponding to a geometric distribution and $\xi = \infty$ a Poisson distribution. Using this framing, we consider how positive correlations between susceptibility and transmissibility impact the speed of transmission as the susceptible population is depleted. [**SJB:** *check overdispersion definitions! Famoye suggests overdispersion with $m_t > 0$, does this line up with what is in text? (If not - how is Famoye's defn converted to what we use? I suggest using ξ to denote the overdispersion parameter*] [**JDH:** *dispersion parameter $\xi = 1/m$ so that $\xi = m = 1$ is geometric, $\xi < 1$ ($m > 1$) is overdispersed, and $\xi \to \infty$ ($m \to 0$) is Poisson distributed.*]

D Model parameters

For all figures, except for Figure 5 which shows the reproduction number as a function of correlation coefficient, we set $\mathcal{R}_0$ =2.0, a value representative of several respiratory viruses such as flu and SARS. We assume that the average time to recovery is 10 days and is exponentially distributed so that the recovery rate is given by $\gamma = 1/10$. Hence, we set $\beta = 0.2$, with the exception of Figure 7-Figure 9 where β is adjusted to compensate for the effects of correlations (between susceptibility (ε) and transmissibility (δ)) and therefore, match the effective exponential growth rate of the epidemics across simulations. The model parameters (descriptions, values, and ranges, thereof) are shown in Table D1.

Table D1. Epidemiological model parameters. Epidemic parameters and distribution parameters explored in models with individual traits of susceptibility (ε) and transmissibility (δ), with $\bar{\varepsilon}(0) = \bar{\delta}(0) = 1$. Baseline values refer to those used in the reference SIR model. Ranges indicate that these parameters vary based on initial conditions which depend on the correlation coefficient. Specific parameter values are noted in Figures.

Parameter	Baseline value	Values explored	Description
$\mathcal{R}_0$	2.0	1.5 to 2.5	Basic reproduction number
γ	1/10 day^{-1}	1/10 day^{-1}	Recovery rate
β	0.2	0.165 to 0.254 day^{-1}	Transmission rate of infections
$\sigma_\varepsilon^2(0)$	0	0.15 to 0.50	Initial variance in susceptibility
$\sigma_\delta^2(0)$	0	0.05 to 0.35	Initial variance in potential transmissibility
ρ	NA	-0.60 to 0.60	Correlation between susceptibility and potential transmissibility

E Simulation methods

All simulations and analysis were performed using MATLAB (version 2023b and 2024a). All simulation code is available at https://github.com/Jeremy-D-Harris/SIR_heterogeneity_project and archived on Zenodo (Harris et al., 2024).

E.1 Deterministic simulations

To approximate the continuous susceptibility and transmissibiliy model variables, we use discrete variables composed of 100 uniformly spaced values between 0 and 6, such that the initial joint distributions we consider are seeded onto a uniform mesh of size 100×100. In visualization of the initial joint distributions we show only the range $\in ([0,3],[0,3])$, which represents $\approx 90\%$ of the population. In all cases, distributions are chosen such that the initial population average susceptibility ($\bar{\varepsilon}$) and potential transmissibility ($\bar{\delta}$) are equal to 1. Epidemic model simulations were numerically integrated using `ode45` in MATLAB (Dormand & Prince, 1980; Shampine & Reichelt, 1997).

To implement initial conditions, we first create the initial joint distributions of ε and δ in the S, I, and R classes (see Appendix C). In all simulations except for in Figure 6, we let the total population be $N = 1$, as in Rose et al., 2021 and let the total population initial conditions be: $S = N$, $I = 0$, $R = 0$, with a small perturbation in the direction of the eigenvector of the SIR model. (Adjusting the perturbation magnitude translates the dynamics in time.) The initial conditions that are passed into the `ode45` function are calculated from Equation 1 - Equation 3.

E.2 Stochastic simulations

To analyze the outbreak potential of epidemics with different underlying susceptibility and transmissibility characteristics we utilize a stochastic simulation approach using the Gillespie algorithm (Gillespie, 1976, 1977). We initialize simulations with a population of 10,000 whose susceptibility and transmissibility values are seeded with probabilities taken from the joint probability distributions used in discrete model simulations to characterize a representative population with explicit individual-level variation. In each stochastic simulation run, one individual, chosen at random, is designated as the index infection. For each of the initial distributions we analyze (SIR, $\rho = -0.6$, $\rho = 0$, $\rho = 0.6$) we run the stochastic simulation 1,000 times to obtain ensembles of epidemic trajectories; and denote a threshold of 50 infections to represent the occurrence an outbreak.